Journal of South American Earth Sciences 97 (2020) 102242

Contents lists available at ScienceDirect

Journal of South American Earth Sciences

journal homepage: www.elsevier.com/locate/jsames

Cretaceous-Cenozoic growth of the Patagonian broken foreland basin, Argentina: Chronostratigraphic framework and provenance variations during transitions in Andean subduction dynamics

Kristina L. Butler[a,b,*], Brian K. Horton[a,b], Andrés Echaurren[c], Andrés Folguera[c], Facundo Fuentes[d]

[a] Department of Geological Sciences, Jackson School of Geosciences, University of Texas at Austin, Austin, TX, USA
[b] Institute for Geophysics, Jackson School of Geosciences, University of Texas at Austin, Austin, TX, USA
[c] Instituto de Estudios Andinos, Facultad de Ciencias Exactas y Naturales, Universidad de Buenos Aires-CONICET, Buenos Aires, Argentina
[d] YPF S.A., 515 Macacha Güemes, Buenos Aires, Argentina

ARTICLE INFO

Keywords:
Andes
Patagonia
Foreland basin
Provenance
U-Pb geochronology
Hf isotopes

ABSTRACT

The Cretaceous-Cenozoic evolution of the Patagonian broken foreland basin system at 42–43°S in the northern Chubut province of Argentina is associated with variable retroarc phases of fold-thrust belt shortening, extension, and basement uplift during changes in the dynamics of oceanic slab subduction. Basement inheritance and progressive shallowing of an east-dipping subducting slab are important mechanisms of foreland partitioning, as dictated by the preexisting (pre-Andean) structural architecture and forelandward (eastward) advance of Late Cretaceous arc magmatism. Previously recognized growth strata help define the timing of fold-thrust belt shortening and retroarc basement-involved uplift, but the precise consequences for sediment routing remain poorly understood, with uncertainties in patterns of basin evolution before, during, and after shallowing and resteepening of the subducting slab.

In this study, distinctive sediment source regions and magmatic histories enable evaluation of the stratigraphic and tectonic evolution of the retroarc foreland basin using new provenance results, maximum depositional ages, and isotopic signatures from detrital zircon U-Pb geochronology and Lu-Hf geochemical analyses. A compilation of published bedrock crystallization ages and distributions of metamorphic and igneous basement rocks identify: a western source region defined by the Andean magmatic arc and associated pre-Andean basement; and an eastern source region consisting of intraplate magmatic units and the North Patagonian Massif.

We demonstrate that Aptian-Cenomanian retroarc basin fill was derived principally from the basement massif and intraplate volcanic units to the east, followed by a Late Cretaceous (Campanian-Maastrichtian) reversal in sedimentary polarity and subsequent exclusive derivation from the Andean arc and orogenic belt to the west. Late Cretaceous-Paleocene slab shallowing and arc cessation was succeeded by late Eocene–earliest Miocene extension during slab rollback and renewal of arc magmatism. Thereafter, Miocene sedimentation was closely linked to shortening in the Andean fold-thrust belt. Within the retroarc succession, new U-Pb ages provide estimates of depositional ages for Lower Cretaceous through Miocene stratigraphic units.

Finally, in addition to U-Pb provenance and chronostratigraphic constraints, zircon Hf isotopic signatures from the detrital record provide confirmation of a Cretaceous-Cenozoic history involving: (1) initial establishment of a continental magmatic arc; (2) transition from a neutral to compressive tectonic regime; (3) shallowing of the subducting slab and arc cessation during retroarc basement partitioning; (4) arc retreat and foreland basin abandonment during slab rollback (with modest extension and crustal thinning); and (5) final renewed shortening during arc rejuvenation.

1. Introduction

The Andean retroarc foreland of northern Patagonia (Fig. 1) records a complex Mesozoic-Cenozoic history of subduction-related contractional, extensional, and neutral tectonic regimes during variable phases of basin genesis, arc magmatism, and convergent-margin geodynamics. The Patagonian broken foreland is situated between two well-studied Andean foreland basins, the Neuquén basin to the north

* Corresponding author. Department of Geological Sciences, Jackson School of Geosciences, University of Texas at Austin, Austin, TX, USA.
E-mail address: kristina.butler@utexas.edu (K.L. Butler).

https://doi.org/10.1016/j.jsames.2019.102242
Received 9 January 2019; Received in revised form 6 June 2019; Accepted 21 June 2019
Available online 25 June 2019

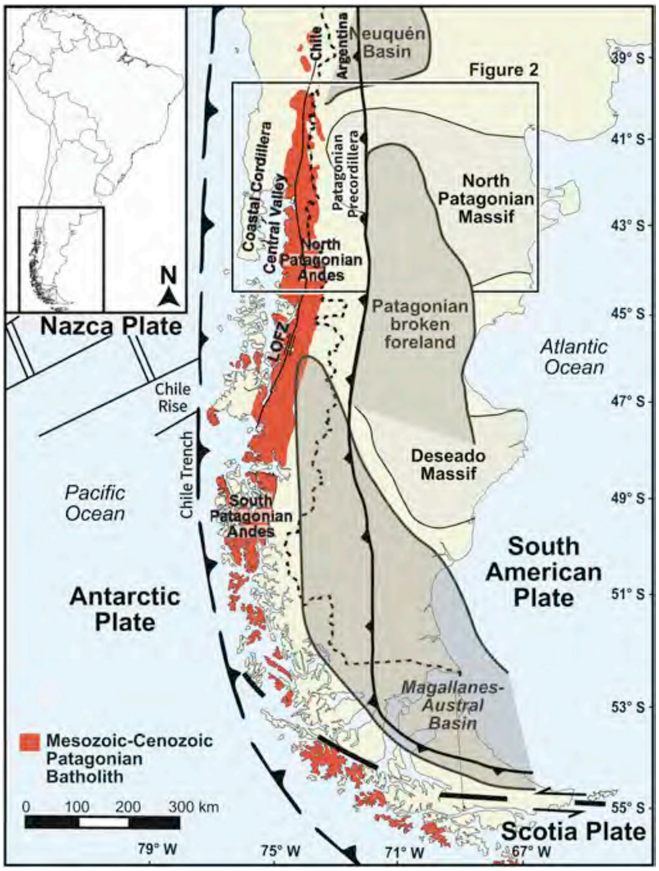

Fig. 1. Simplified regional map of southern South America showing sedimentary basins (Neuquén Basin, Patagonian broken foreland, and Magallanes-Austral Basin), basement provinces (North Patagonian Massif and Deseado Massif), modern tectonic plate boundaries (Nazca, Antarctic, South American, and Scotia plates), and key orogenic elements (from west to east, the Chile Rise, Chile trench, Coastal Cordillera, Central Valley, Liquiñe-Ofqui fault zone (LOFZ), North Patagonian Andes, South Patagonian Andes, deformation front of the North Patagonian fold-thrust belt (teeth), and Patagonian Precordillera).

and the Magallanes-Austral basin to the south (Horton, 2018a and references therein), and is bordered by large basement provinces defined by the Deseado and North Patagonian massifs. The basement massifs and adjacent broken foreland region (Fig. 1) preserve important records of deformation, magmatism, and sedimentation before and during Andean orogenesis (Franzese et al., 2003; Pankhurst et al., 2006; Ramos, 2008). Inherited structures accommodated Andean shortening in both hinterland and retroarc regions through the reactivation of basement-involved faults and inversion of former extensional basins (Giacosa and Heredia, 2004; Echaurren et al., 2016). Contrasting phases of shortening and extension are likely linked to differences in coupling of the downgoing and overriding plates during shallowing and resteepening of the subducting slab (Horton and Fuentes, 2016; Horton, 2018b), as expressed in the irregular Late Cretaceous inboard advance, Paleocene-middle Eocene cessation, and middle-Eocene–Miocene trenchward retreat and broadening of arc magmatism (Folguera and Ramos, 2011; Gianni et al., 2018). Episodes of Paleocene-Eocene intraplate volcanism may be related to slab window genesis or lithospheric removal (Muñoz et al., 2000; de Ignacio et al., 2001; Aragón et al., 2011b, 2013; Kay et al., 2007; Zaffarana et al., 2012; Iannelli et al., 2018).

The Andean history of the North Patagonian region involved the development of a fold-thrust belt (Giacosa and Heredia, 2004; Giacosa et al., 2005; García Morabito and Ramos, 2012), structural partitioning of the adjacent foreland basin (Bilmes et al., 2013; Gianni et al., 2015; Echaurren et al., 2016; Savignano et al., 2016; Franzese et al., 2018), and evolution of the magmatic arc linked to variations in slab dip (Pankhurst et al., 1999; Suárez and de la Cruz, 2001; Folguera and Ramos, 2011; Echaurren et al., 2016, 2017; Gianni et al., 2018; Folguera et al., 2018a, 2018b; Fernández Paz et al., 2018). However, most of the prevailing tectonic models have been proposed on the basis of structural and magmatic records, with limited information regarding sedimentary basin dynamics (i.e., timing of deposition, duration of stratigraphic hiatuses, and potential shifts in sedimentary provenance). Such information would shed light on basin generation mechanisms in the context of the previously proposed tectonic framework for this segment of the Andean margin, with implications for alternating tectonic regimes (shortening, extension, and stasis), continental crustal budgets (crustal thickening and thinning), subduction dynamics (slab shallowing and resteepening), and magmatic arc behavior (advance, retreat, cessation, and rejuvenation).

Here we integrate regional stratigraphic and geologic constraints with new detrital zircon U-Pb geochronological results for 14 samples from Cretaceous-Cenozoic retroarc successions that span proposed phases of slab shallowing and resteepening in the northern segment (42–43°S) of the Patagonian broken foreland basin (Fig. 2). These data provide insights into provenance variations during shifts in deformational mode within the overriding plate, as well as new chronostratigraphic constraints for Cretaceous through Neogene basin fill (Fig. 3). We also evaluate the Lu-Hf isotope geochemistry of 4 detrital zircon samples to investigate crustal evolution trends over a broad period (~200–10 Ma) encompassing several transitions in subduction dynamics. Our results point to a first-order control of Andean orogenesis and subduction processes on sediment source regions, including a change from an eastern basement source to a western Andean source during proposed Late Cretaceous slab shallowing. Moreover, crustal evolution trends in the North Patagonian retroarc region reflect fluctuating tectonic regimes that define contrasting stages of basin evolution linked to variable extension and shortening.

2. Geologic setting

2.1. Modern configuration

The Andean orogenic profile across northern Patagonia (Fig. 1) includes a western forearc region (Coastal Cordillera and Central Valley), the Andean magmatic arc (North Patagonian Andes), a relatively low elevation (< 2 km) fold-thrust belt (Patagonian Precordillera), and a wide (~400 km) foreland partitioned by basement-involved structures (Patagonian broken foreland basin) in the east. The North Patagonian Andes are situated north of the Nazca-Antarctic-South American triple junction at ~46.5°S, where the Chile Rise spreading center intersects the trench. The Liquiñe-Ofqui fault zone (LOFZ) is a continuous (~1000 km long) intra-arc right-lateral strike-slip fault that accommodated oblique convergence and enhanced Neogene-Quaternary magmatism and denudation (Hervé, 1994; Thomson, 2002; Adriasola et al., 2005). The Patagonian broken foreland basin is flanked by two basement provinces, the North Patagonian (or Somún Cura) massif and the Deseasdo massif, and is situated between two well-studied Andean retroarc foreland basins, the Neuquén basin to the north and the Magallanes-Austral basin to the south (e.g., Biddle et al., 1986; Howell et al., 2005; Romans et al., 2011; Fosdick et al., 2011; Ghiglione et al., 2010; Balgord and Carrapa, 2016; Horton et al., 2016; Schwartz et al., 2017).

2.2. Retroarc foreland basin

The Patagonian broken foreland (Fig. 2) hosts a Lower Cretaceous through Miocene clastic succession punctuated by two depositional hiatuses and extensive igneous units (Fig. 3). The nonmarine Lower Cretaceous Chubut Group comprises principally fluvial deposits with local volcaniclastic facies and is divided into the Los Adobes and Cerro

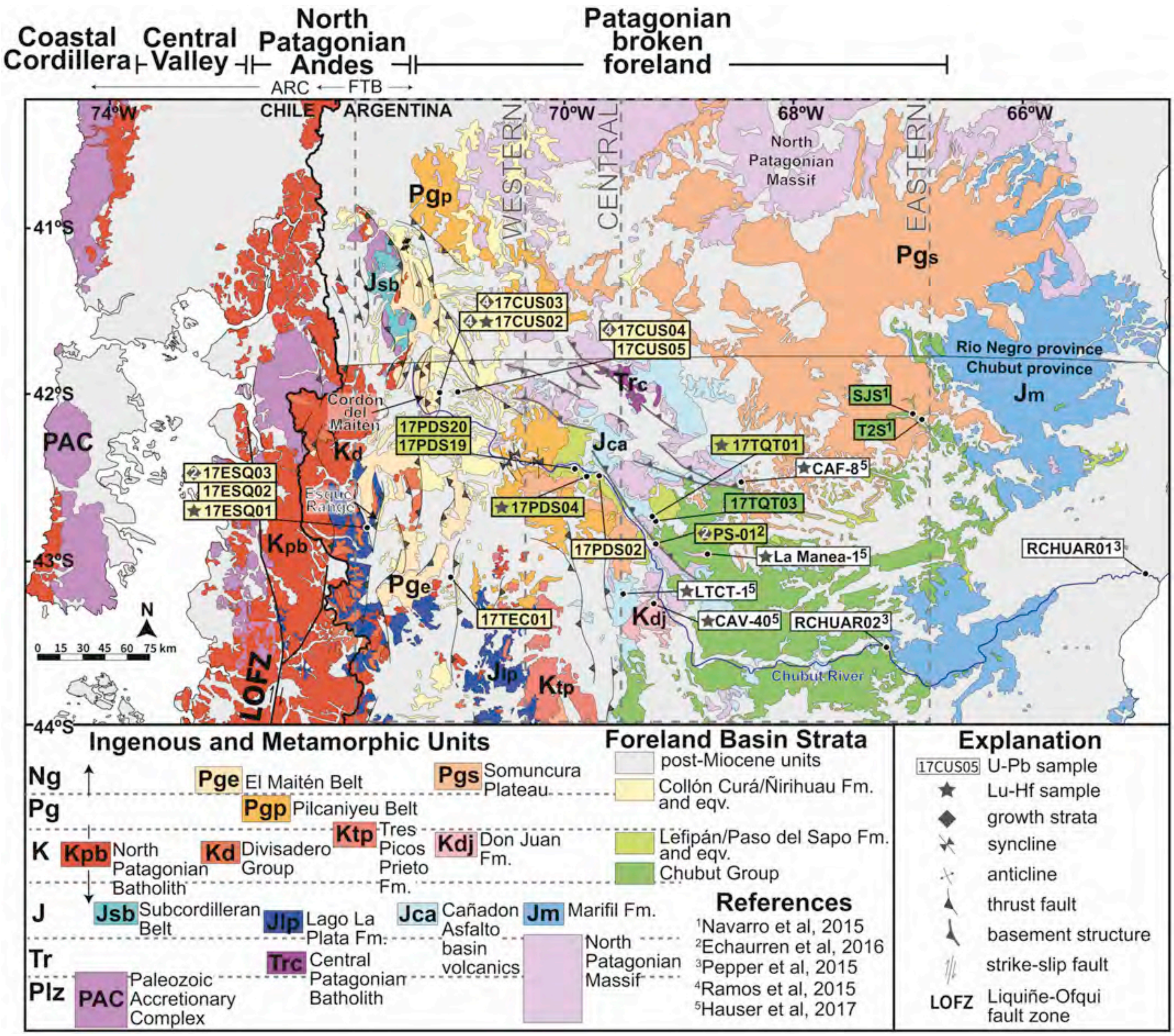

Fig. 2. Geologic map of northern Patagonia depicting major structures, sample and growth strata localities (after Ardolino et al., 1998; and Lizuaín and Viera, 2010). Corresponding chart shows the names of geologic units of variable age: Paleozoic (Pz), Triassic (Tr), Jurassic (J), Cretaceous (K), Paleogene (Pg), and Neogene (Ng).

Barcino Formations (Marveggio and Llorens, 2013; Figari et al., 2015; Suárez et al., 2014; Navarro et al., 2015). A depositional hiatus separates the Chubut Group from the overlying marginal marine Upper Cretaceous-lower Paleogene Paso del Sapo and Lefipán Formations (Spalletti, 1996; Scasso et al., 2012). Locally, the Paso del Sapo Formation directly overlies igneous rocks of the Jurassic Cañadon Asfalto Basin volcanics. An additional depositional hiatus, of late Paleocene–Oligocene age, is coeval with volcanic emplacement of the Pilcaniyeu Belt (Huitrera Formation) and El Maitén Belt (Ventana Formation; Rapela et al., 1988; Aragón et al., 2011b, 2013). The youngest basin fill of the Patagonian broken foreland (Fig. 3) unconformably overlies the Paso del Sapo-Lefipán sedimentary succession and Huitrera-Ventana volcanic deposits, and is composed of Miocene fluvial, lacustrine, and alluvial-fan deposits of the Ñirihuau, La Pava, and Collón Curá Formations (Bilmes et al., 2014; Bechis et al., 2014; Echaurren et al., 2016; Bucher et al., 2018).

2.3. Retroarc basement

Crystalline basement of northern Patagonia (Figs. 1 and 2) consists of Paleozoic-Mesozoic metamorphic complexes and igneous suites (Fig. 4). Metamorphic basement is exposed on the eastern flank of the North Patagonian Andes within the fold-thrust belt (~41–42°S, Colohuincul Complex; Hervé et al., 2018). In the retroarc zone, the North Patagonian Massif defines a broad and discontinuous region (~71-66°W) of Paleozoic-Triassic metamorphic and igneous basement units (Figs. 2 and 4). This massif is capped by a voluminous Jurassic rhyolitic ignimbrite (V1 volcanic stage deposits of the Marifil Formation; Pankhurst et al., 2000, 2006). Prior to the main phase of Andean shortening, prolonged Late Triassic–Early Cretaceous extension was associated with Gondwanan breakup and opening of the South Atlantic (Franzese et al., 2003; Ramos, 2009). Mesozoic normal faults bounding extensional basins (e.g., the Early Jurassic Cañadón Asfalto Basin; Hauser et al., 2017) were later inverted during Andean shortening in hinterland and foreland regions (Bilmes et al., 2013; Echaurren et al., 2016).

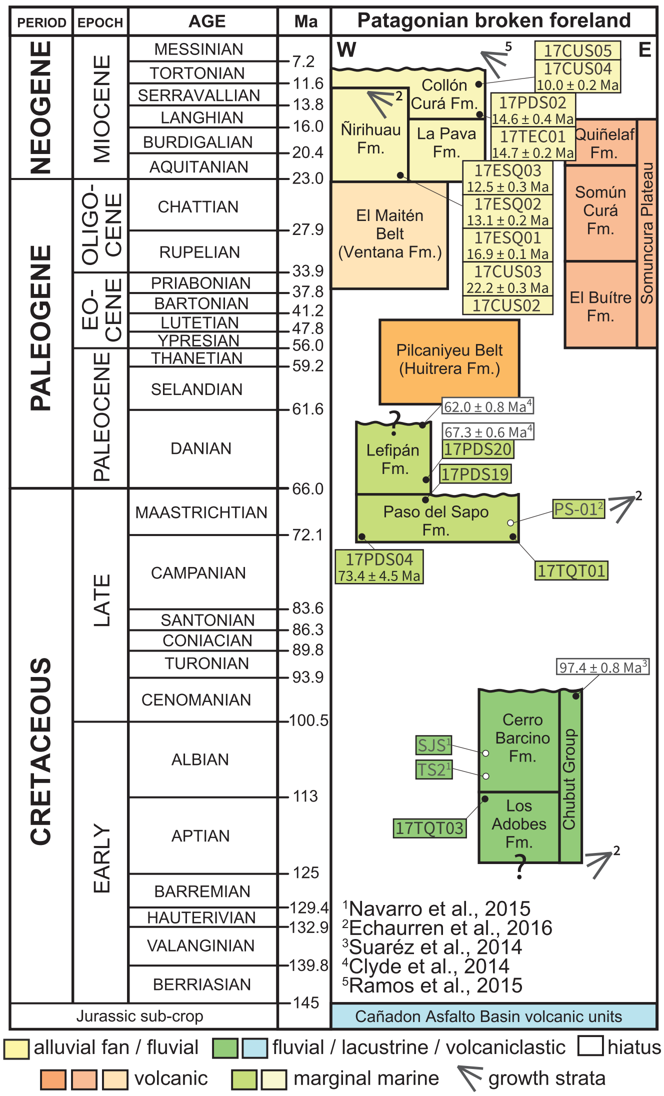

Fig. 3. Cretaceous-Paleogene-Neogene stratigraphic chart for the Patagonian broken foreland showing stratigraphic units and sampled stratigraphic level, growth strata intervals, hiatuses, unconformities, and maximum depositional ages. Timescale after Cohen et al. (2018).

2.4. Fold-thrust belt

The North Patagonian fold-thrust belt (Figs. 1 and 2) is a narrow (< 100 km), low-elevation (< 2 km) basement-involved zone of dominantly east-directed thrust faults and subordinate west-directed back-thrusts (Giacosa and Heredia, 2004). The decollement is rooted in pre-Mesozoic basement at ~15 km depth (Colohuincul Complex; Echaurren et al., 2016). Total shortening did not exceed ~20 km (< 16%, Orts et al., 2015). Thrust sheets involve Jurassic-Cretaceous arc-related plutonic rocks (North Patagonian Batholith and the Subcordilleran Belt), Jurassic sedimentary and volcanic units (Pilquitrón Formation), and Cenozoic volcanic rocks of the Paleocene-Eocene Pilcaniyeu Belt (Huitrera Formation) and Eocene-lowermost Miocene El Maitén Belt (Ventana Formation). The hinterland recorded two phases of shortening (Cretaceous-Paleocene and Miocene) and an intervening period of extension (Oligocene-earliest Miocene). The earliest episode of shortening is recognized as Aptian-Albian, as defined by an angular unconformity between Lower Jurassic units and the overlying Cretaceous Divisadero Group (Suárez et al., 2009b; 2010; Echaurren et al., 2016, 2017). Oligocene-early Miocene extension across forearc and retroarc regions at 40-42°S is recognized by a strong positive gravity anomaly and seismically imaged low-angle normal faults (Spalletti and Dalla Salda, 1996; Muñoz et al., 1998; Jordan et al., 2001). The main phase of shortening and fold-thrust belt development is constrained to the middle-late Miocene by apatite fission-track cooling ages and growth strata involving the Collón Curá and Ñirihuau Formations (Fig. 3; Thomson et al., 2001; Giacosa and Heredia, 2004; Ramos et al., 2015).

2.5. Magmatic arc

In northern Patagonia, the Andean magmatic arc (Figs. 1 and 2) is composed of the calc-alkaline North Patagonian Batholith (41–46°30′S) and its volcanic equivalents (Fig. 4). Granitic suites intruded progressively shallower crustal levels from Late Jurassic to late Miocene time, with a main phase of mid-Cretaceous emplacement broadly coincident with early Andean shortening (~135-80 Ma, Pankhurst et al., 1999; Suárez and de la Cruz, 2001; Adriasola et al., 2005; Aragón et al., 2011a; Castro et al., 2011).

3. Sediment source regions

A compilation of published isotopic ages and detrital zircon age distributions for crystalline bedrock and metamorphic units (Fig. 4) characterizes sediment source regions for the Cretaceous–Neogene Patagonian broken foreland, including western sources (North Patagonian Andes) and eastern sources (North Patagonian Massif and Mesozoic-Cenozoic intraplate volcanic units).

3.1. Basement

Basement rocks crop out in the both the western hinterland (including a Paleozoic accretionary complex, Colohuincul Complex, and Devonian intrusive rocks) and eastern retroarc region (the North Patagonian Massif consisting of Paleozoic metamorphic rocks and Paleozoic-Mesozoic plutonic suites). These basement units yield a broad range of overlapping Paleozoic ages, with common age peaks centered around 530-520, 475-465, 400-390, 375-365, 330-320, 290-280, and 260-250 Ma (Fig. 4B).

3.2. Magmatic arc units

Mesozoic-Cenozoic subduction along the western margin of South America produced magmatic arc plutonic suites and volcanic equivalents (Figs. 2 and 4). The oldest of these is the Late Triassic Central Patagonian Batholith (~222-206 Ma), a NW-trending granitic belt exposed within the modern foreland (Rapela et al., 1992; Zaffarana et al., 2014). The Early Jurassic Subcordilleran Belt (~185-181 Ma) is a NNW-trending granitic belt exposed within the Andean fold-thrust belt (Rapela et al., 2005). The granitic North Patagonian Batholith (~173–5 Ma) recorded much of the Cretaceous-Cenozoic activity of the Andean magmatic arc (González Díaz, 1982; Pankhurst et al., 1994; Pankhurst et al., 1999; Rolando et al, 2002, 2004; Aragón et al., 2011a; Castro et al., 2011). Volcanic equivalents of the North Patagonian Batholith include: dacitic-rhyolitic ignimbrites and associated pyroclastic products of the Lago la Plata Formation (~153-136; Suárez et al., 2009a); the andesitic-dacitic-rhyolitic Divisadero Group (~118-105 Ma; Suárez et al., 2009b, 2010; Aragón et al., 2011a; Echaurren et al., 2017), andesitic-dacitic Don Juan Formation (~91 Ma; Franchi and Page, 1980); recently identified calc-alkaline dacites near Gastre (~76-74 Ma; Zaffarana et al., 2018); and the subalkaline to tholeiitic El Maitén Belt (~37-20 Ma; Fernández Paz et al., 2018; Rapela et al., 1988; Bechis et al., 2014). The Lago la Plata Formation, Divisadero Group and El Maitén Belt are exposed today along the eastern slope of the North Patagonian Andes and into the foreland region at ~72-70°W. The Don Juan Formation and Gastre dacites crop out farther east in the foreland domain.

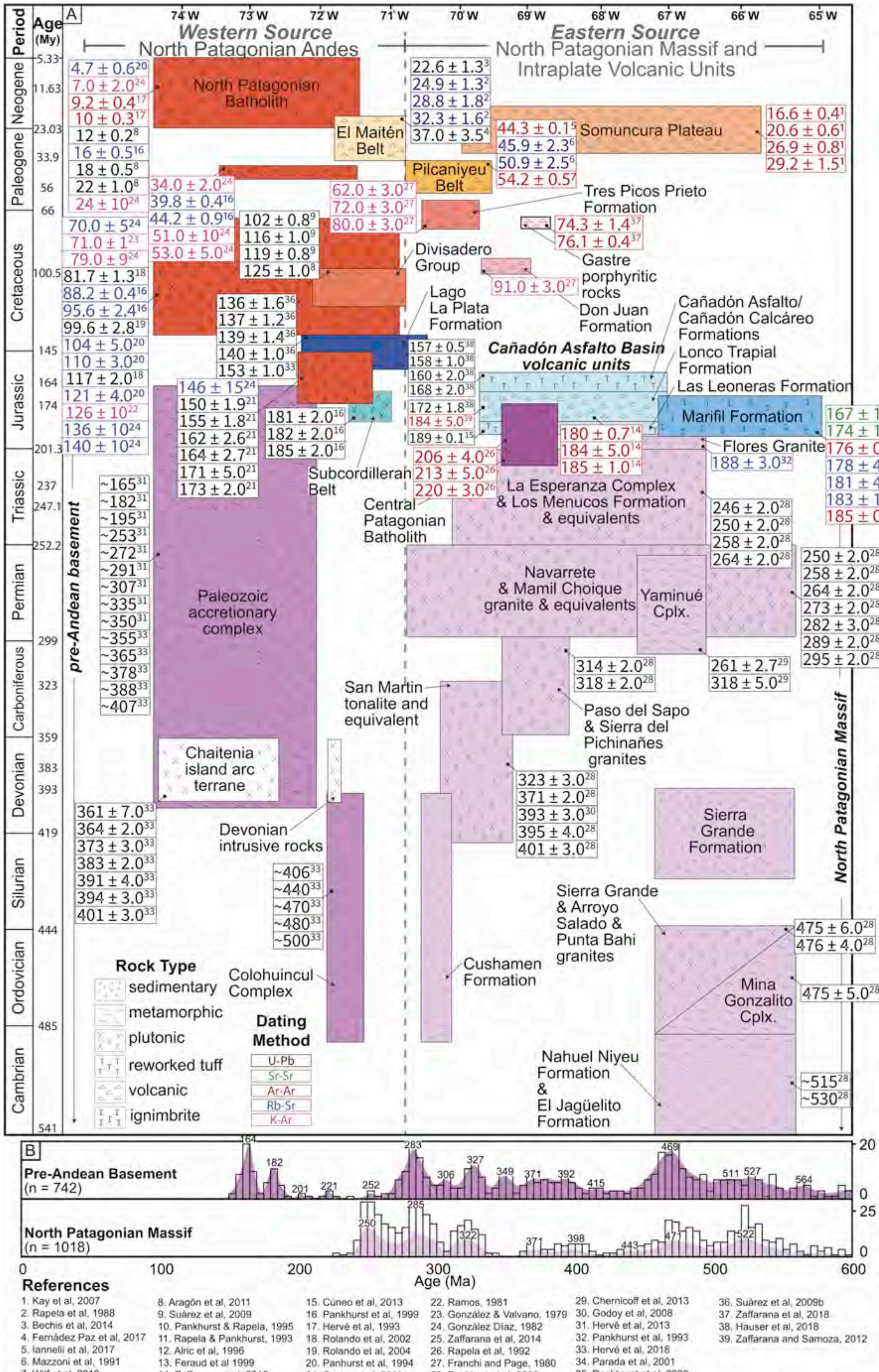

(caption on next page)

Fig. 4. (A) Phanerozoic stratigraphic chart for western and eastern sediment source regions in northern Patagonia at ~40–44°S showing the name, age, and lithology of various geologic units, including published isotopic ages. (B) Plots of the composite age distributions for basement units of the western source region (pre-Andean basement) and eastern source region (North Patagonian Massif) showing probability density plots (shaded colors) and age histograms (thin rectangles), with bold numerals identifying age peaks (in Ma).

3.3. Intraplate volcanic units

Two major intraplate volcanic provinces were emplaced during the Jurassic: (1) the rhyolitic ignimbrites of the Marifil Formation which are exposed extensively along the Atlantic margin (~185-167 Ma; Pankhurst and Rapela, 1995; Alric, 1996; Pankhurst et al., 2000); and (2) the volcanic and volcaniclastic units of the NW-trending Cañadón Asfalto extensional basin, these include the Cañadón Calcareo (~157 Ma), Cañadón Asfalto (~168-158 Ma), Lonco Trapial (~180-172 Ma), and Las Leonares (~185-180 Ma) Formations (Cúneo et al., 2013; Hauser et al., 2017). Intraplate volcanic units of latest Cretaceous-Cenozoic age crop out across the modern foreland region east of the North Patagonian Andes. These units include Late Cretaceous basalts of the Tres Picos Prieto Formation (~80-62 Ma; Franchi and Page, 1980), the Paleocene-Eocene Pilcaniyeu Belt (~60-42 Ma; Mazzoni et al., 1991; Wilf et al., 2010; Iannelli et al., 2017), and the Oligocene-Miocene Somuncura Plateau (~33-16 Ma; Kay et al., 2007).

3.4. Western versus eastern sediment source regions

To investigate when the Andean hinterland became the dominant sediment source to the retroarc region, we delineate two sediment source regions defined by the ~71°W boundary between the North Patagonian Andes and the modern Patagonian broken foreland basin (Figs. 2 and 4).

In the west, the Andean domain includes the magmatic arc, fold-thrust belt, and pre-Andean basement, largely defined by rocks of the North Patagonian Batholith, Divisadero Group, Lago la Plata Formation, and El Maitén Belt. On the eastern Andean flank, the Subcordilleran Belt and Devonian plutonic units intrude metamorphic units of the Paleozoic Colohuincul Complex. On the western Andean flank, the Paleozoic accretionary complex hosts Devonian intrusive rocks of the Chaitenia island arc terrane (~400–360 Ma; Hervé et al., 2013, 2016, 2018). A composite age distribution compiled from > 740 published zircon U-Pb analyses (Fig. 4B) reveals a broad range of Precambrian to Jurassic age grains within pre-Andean basement. The most diagnostic age ranges from the North Patagonian Andes come from the North Patagonian Batholith, with clusters of ~140-80 Ma and < 20 Ma ages.

The eastern domain includes extensive intraplate volcanic units (Marifil Formation, Tres Picos Prieto Formation, Pilcaniyeu Belt, Somuncura Plateau, Cañadón Asfalto Basin volcanic rocks), North Patagonian massif basement units, and subordinate exposures of magmatic arc units (Central Patagonian Batholith, Don Juan Formation, Gastre porphyritic rocks). Diagnostic age ranges include early Pilcaniyeu volcanic rocks (~60-55 Ma) and the Marifil Formation (~188-172 Ma). It is important to note that the Marifil Formation ignimbrite and plutonic Subcordilleran Belt overlap in age. However, structural, thermochronologic, and shortening-related growth stratal relationships indicate exhumation of the Andean fold-thrust belt during middle-late Miocene time (Thomson et al., 2001; Giacosa and Heredia, 2004; Ramos et al., 2015; Manuel López et al., 2019), suggesting the Subcordilleran Belt was not exposed as a potential sediment source until Neogene time.

4. Methods

Fourteen fine- to medium-grained sandstone samples were collected from Cretaceous–Neogene strata across the northern Chubut province of Argentina from eastern (Lower Cretaceous), central (Upper Cretaceous), and western (Neogene) segments of the Patagonian broken foreland (Table 1). All 14 samples were analyzed for detrital zircon U-

Table 1
Summary table listing sample location, formation, stratigraphic position and analyses.

Broken foreland segment	Sample	Group	Formation	Position	Latitude	Longitude	Reference	Analyses
Eastern	17TQT03	Chubut Group	Los Adobes	uppermost	-42.95695	-69.22085	this study	DZ U-Pb
	SJS	Chubut Group	Cerro Barcino	unknown			Navarro et al., 2015	
	TS2	Chubut Group	Cerro Barcino	unknown			Navarro et al., 2015	
Central	17PDS04		Paso del Sapo	base	-42.68170	-69.75127	this study	DZ U-Pb/Lu-Hf
	17TQT01		Paso del Sapo	base	-42.91861	-69.25062	this study	DZ U-Pb/Lu-Hf
	17PDS19		Paso del Sapo	top	-42.66920	-69.85631	this study	DZ U-Pb
	PS-01		Paso del Sapo	unknown			Echaurren et al., 2017	
	17PDS20		Lefipán	base	-42.66920	-69.85631	this study	DZ U-Pb
Western	17ESQ01		Ñirihuau	lower	-42.85589	-71.33666	this study	DZ U-Pb/Lu-Hf
	17CUS02		Ñirihuau	lower	-42.07128	-71.02575	this study	DZ U-Pb/Lu-Hf
	17CUS03		Ñirihuau	lower	-42.07128	-71.02575	this study	DZ U-Pb
	17ESQ02		Ñirihuau	upper	-42.98508	-71.48938	this study	DZ U-Pb
	17ESQ03		Ñirihuau	upper	-42.98508	-71.48938	this study	DZ U-Pb
	17CUS04		Collón Curá	upper	-42.09754	-70.91980	this study	DZ U-Pb
	17CUS05		Collón Curá	upper	-42.09754	-70.91980	this study	DZ U-Pb
	17TEC01		Collón Curá	lower	-43.39247	-70.74107	this study	DZ U-Pb
	17PDS02		La Pava	lower	-42.68313	-69.66150	this study	DZ U-Pb

Pb geochronology and four of these were analyzed for Lu-Hf-Yb isotopic values (Figs. 2 and 3). Following conventional physical and chemical mineral density separation techniques (including water table, heavy liquid and magnetic separation), a random selection of inclusion-free zircon grains of variable size and shape were analyzed for U-Pb geochronology on the Element 2 HR ICPMS (inductively coupled plasma mass spectrometer), with subsequent Lu-Hf-Yb isotope analyses on the Nu Plasma HR multicollector ICPMS at the University of Arizona LaserChron Center. U-Pb and Lu-Hf-Yb analyses follow techniques defined by Gehrels et al. (2006, 2008), Gehrels and Pecha (2014), and Cecil et al. (2011). We report U-Pb geochronological results with measured age uncertainties of 1–2% (1σ error) and present results for individual samples as maximum depositional ages (MDA; Fig. 5) and probability density functions (Fig. 6). We use $^{206}Pb/^{238}U$ ages for zircons younger than 900 Ma and $^{206}Pb/^{207}Pb$ ages for zircons older than 900 Ma. Individual analyses were filtered such that results displaying > 20% discordance, > 5% reverse discordance, or 10% internal uncertainty were discarded. For each sample, 100–125 individual zircon grain ages were obtained. MDAs for individual samples are calculated on the basis of the youngest group of U-Pb ages, and reported as weighted mean ages with 2σ analytical errors (Ludwig, 2008). In reporting MDAs, we consider the youngest single grain, the youngest age peak, and the youngest population of grains overlapping at 2σ (2+ grains) for each sample (Dickinson and Gehrels, 2009). Given the proximity of the Andean magmatic arc, it is likely that some samples contain syndepositional volcanogenic zircons and therefore some MDAs may represent approximations of the true depositional age (e.g., Dickinson and Gehrels, 2009; Horton et al., 2015; Schwartz et al., 2017; Daniels et al., 2017). Hf isotopic results are reported in epsilon units (ε) and presented in Hf evolution diagrams (Fig. 7) as εHf(t) values representing the isotopic composition at the time of crystallization (t) in reference to CHUR (chondritic uniform reservoir; Bouvier et al., 2008), DM (depleted mantle; Vervoort and Blichert-Toft, 1999) and average crustal evolution (assuming modern $^{176}Lu/^{177}Hf = 0.0115$; Vervoort and Patchett, 1996; Vervoort and Blichert-Toft, 1999). Measured $^{176}Hf/^{177}Hf$ uncertainties are ~1 epsilon unit (1ε). Detailed analytical methods, results, and supporting references are provided in the supplementary material (Appendices A-C).

4.1. Eastern segment: lower to mid-Cretaceous samples

The Aptian–Cenomanian Chubut Group is exposed in the eastern segment of the North Patagonian retroarc region (Figs. 2 and 3) and is evaluated here using new and published U-Pb geochronological results. For the lower Chubut Group, a sample was collected from the uppermost Los Adobes Formation near the Taquetrén Range (sample 17TQT03; -42.95695, -69.22085). For the upper Chubut Group, Navarro et al. (2015) presented U-Pb results for the undifferentiated Cerro Barcino Formation near Telsen (samples SJS and TS2).

4.2. Central segment: Upper Cretaceous samples

In the central segment of the Patagonian broken foreland, the Upper Cretaceous-Paleocene Paso del Sapo and Lefipán Formations (Figs. 2 and 3) are characterized by U-Pb results for five samples, listed here in stratigraphic order. Two samples were collected from the basal Paso del Sapo Formation, which locally overlies the Jurassic Cañadon Asfalto Basin volcanic units in the central outcrop belt along the Chubut River (sample 17PDS04: -42.68170, -69.75127) and eastern outcrop belt in the Taquetrén Range (sample 17TQT01; -42.91861, -69.25062). An additional sample from the Taquetrén Range was presented by Echaurren et al. (2016) for interpreted Paso del Sapo growth strata associated with initial shortening in the region (sample PS-01). Samples from the transition from the uppermost Paso del Sapo (17PDS19) to lowermost Lefipán Formation (17PDS20) along the Chubut River (-42.66920, -69.85631) were collected from a stratigraphic section described by Spalletti (1996) and Scasso et al. (2012).

4.3. Western segment: Neogene samples

Neogene deposits of the Collón Curá and Ñirihuau Formations are most prevalent where collected in western segments of the Patagonian broken foreland basin and the adjacent foothills of the North Patagonian Andes (Figs. 2 and 3). Samples from the lowermost Neogene levels were collected from outcrops considered to be the lower Ñirihuau Formation, which directly overlying upper Eocene-Oligocene volcanic rocks in the Esquel Range (17ESQ01: -42.85589, -71.33666) and the Cordón del Maitén (17CUS02 and 17CUS03: -42.07128, -71.02575) of the Andean foothills. From higher stratigraphic levels, samples from separate growth stratal packages (Fig. 7) include the upper Ñirihuau Formation associated with uplift of the Esquel Range (17ESQ02 and 17ESQ03: -42.98508, -71.48938; Echaurren et al., 2016) and the Collón Curá Formation associated with uplift of the Cordón del Maitén near the town of Cushamen (17CUS04 and 17CUS5: -42.09754, -70.91980; Ramos et al., 2015; their samples 13-M2, MR-2, and 13-M4). The lower levels of the regionally extensive Collón Curá Formation were sampled in the west near the Tecka Range (17TEC01: -43.39247, -70.74107) and farther east along the Chubut River near the town of Paso del Sapo (17PDS02: -42.68313, -69.66150; locally La Pava Formation) where it disconformably overlies the Upper Cretaceous Paso del Sapo Formation.

5. Detrital zircon U-Pb geochronological results and interpretations

Sediment provenance patterns and depositional ages for the Patagonian broken foreland basin (Figs. 2 and 3) are assessed using U-Pb geochronological results for the Lower Cretaceous through Neogene succession (Appendices A-C). The results help refine chronostratigraphic age estimates (Fig. 5), identify sediment source regions and changes in sediment routing (Fig. 6), define age of key growth structures (Fig. 7), and clarify crustal evolution patterns (Fig. 8).

5.1. Refined chronostratigraphy and depositional ages

New estimates of maximum depositional age (MDA) are presented for 8 samples from the Cretaceous-Paleogene succession (Fig. 5). The results are summarized here in approximate stratigraphic order for western, central, and eastern segments of the broken foreland region (Tables 1 and 2; Figs. 2 and 3).

For the Cretaceous-Paleocene succession in the central to eastern basin segments, the upper Los Adobes Formation (lower Chubut Group) produced a single youngest grain of Albian age (106.9 ± 2.2 Ma), with

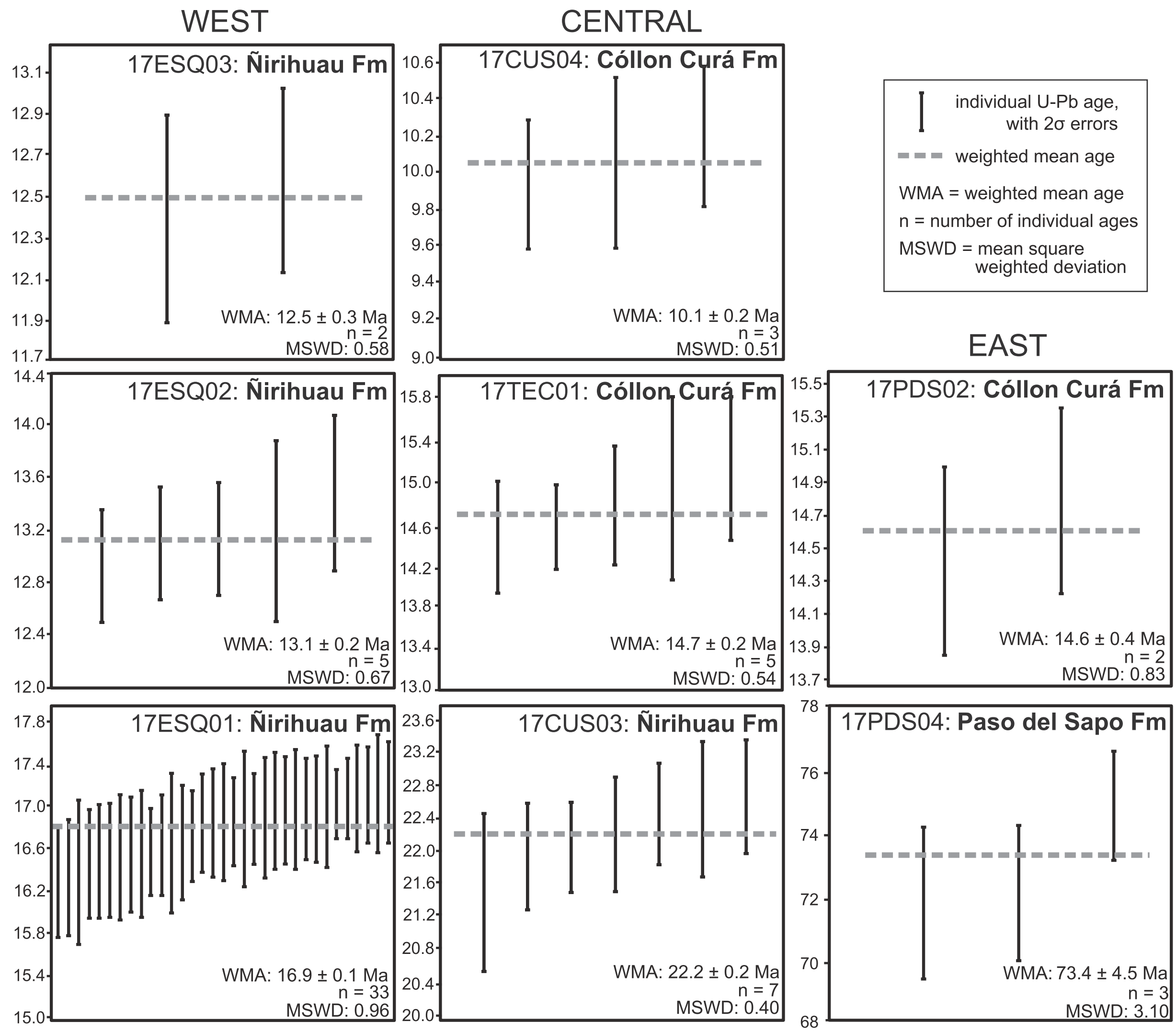

Fig. 5. Plots showing the youngest detrital zircon U-Pb age populations for individual samples. WMA = weighted mean age, MSWD = mean square weighted deviation.

no additional grain ages overlapping within error. Results for the Cerro Barcino Formation presented by Navarro et al. (2015; samples SJS and T2S) also contain Albian grains, with MDAs of 109 ± 2 Ma (SJS) and 106 ± 1.6 Ma (T2S). The basal Paso del Sapo Formation yields an MDA of 73.4 ± 4.5 Ma (sample 17PDS04; n = 3 grains), in accordance with ages of 71.0 ± 2.4 Ma and 71.9 ± 1.8 Ma for the single youngest grains for two additional samples from the Paso del Sapo Formation (17PDS04, 17PDF19). These latest Campanian-Maastrichtian ages all overlap within error and are considerably younger than a previously reported MDA near the Santonian-Campanian boundary of 83.1 ± 1.6 Ma (Echaurren et al., 2016; sample PS-01). Upsection, the overlying Maastrichtian-lower Paleocene Lefipán Formation contains a youngest grain (81.4 ± 1.8 Ma) older than the aforementioned youngest grains from the underlying Paso del Sapo Formation.

Within the Neogene succession, which is best expressed in the Andean foothills and western foreland, new MDAs clarify the depositional ages of the Ñirihuau and Collón Curá Formations (Fig. 5). Near the Cordón del Maitén, a sample from the oldest basin fill provides an MDA of 22.2 ± 0.3 Ma (sample 17CUS3). This sample is from a basal exposure of a clastic succession that directly overlies the late Eocene-Oligocene volcanic rocks of the Ventanta Formation. The early Miocene MDA indicates deposition of the basal Ñirihuau Formation partially coeval with late El Maitén magmatism (∼22 Ma). In the Andean foothills, near Esquel, 3 samples from the better-studied exposures of Ñirihuau Formation yield MDAs, in stratigraphic order, of 16.9 ± 0.1 Ma, 13.1 ± 0.2 Ma, and 12.5 ± 0.3 Ma (samples 17ESQ01, 17ESC02, and 17ESQO3, respectively). The Collón Curá Formation is rich in volcanogenic materials and shows comparable MDAs of 14.7 ± 0.2 Ma and 14.6 ± 0.4 for samples from lower levels in the central (17TEC01) and eastern (17PDS02) basin segments. In the central zone, samples from successively higher stratigraphic levels display an MDA of 10.1 ± 0.2 Ma (17CUS04) followed by a single grain age of 9.3 ± 0.3 Ma (17CUS5).

5.2. Sediment provenance results

Consideration of detrital zircon U-Pb results for all 17 samples, as depicted in a composite probability density plot (Fig. 6), helps delineate 8 major age populations within the Cretaceous-Cenozoic Patagonian broken foreland: ∼410–360 Ma, ∼330–280 Ma, ∼230–210 Ma, ∼200–170 Ma, ∼140–80 Ma, ∼60–50 Ma, ∼40–30 Ma and ∼20–10 Ma. Five of these populations can be assigned to discrete sediment source units, including three major western sources in the North Patagonian Batholith (∼140–80 Ma; < 20 Ma), Subcordilleran Batholith (∼185–180 Ma), and El Maitén Belt (∼37–20 Ma), and two major eastern sources in the Marifil Formation (∼188–172 Ma) and Pilcaniyeu Belt (∼60–42 Ma). The original sources for pre-Jurassic age populations are more ambiguous, as these ages may have originated from

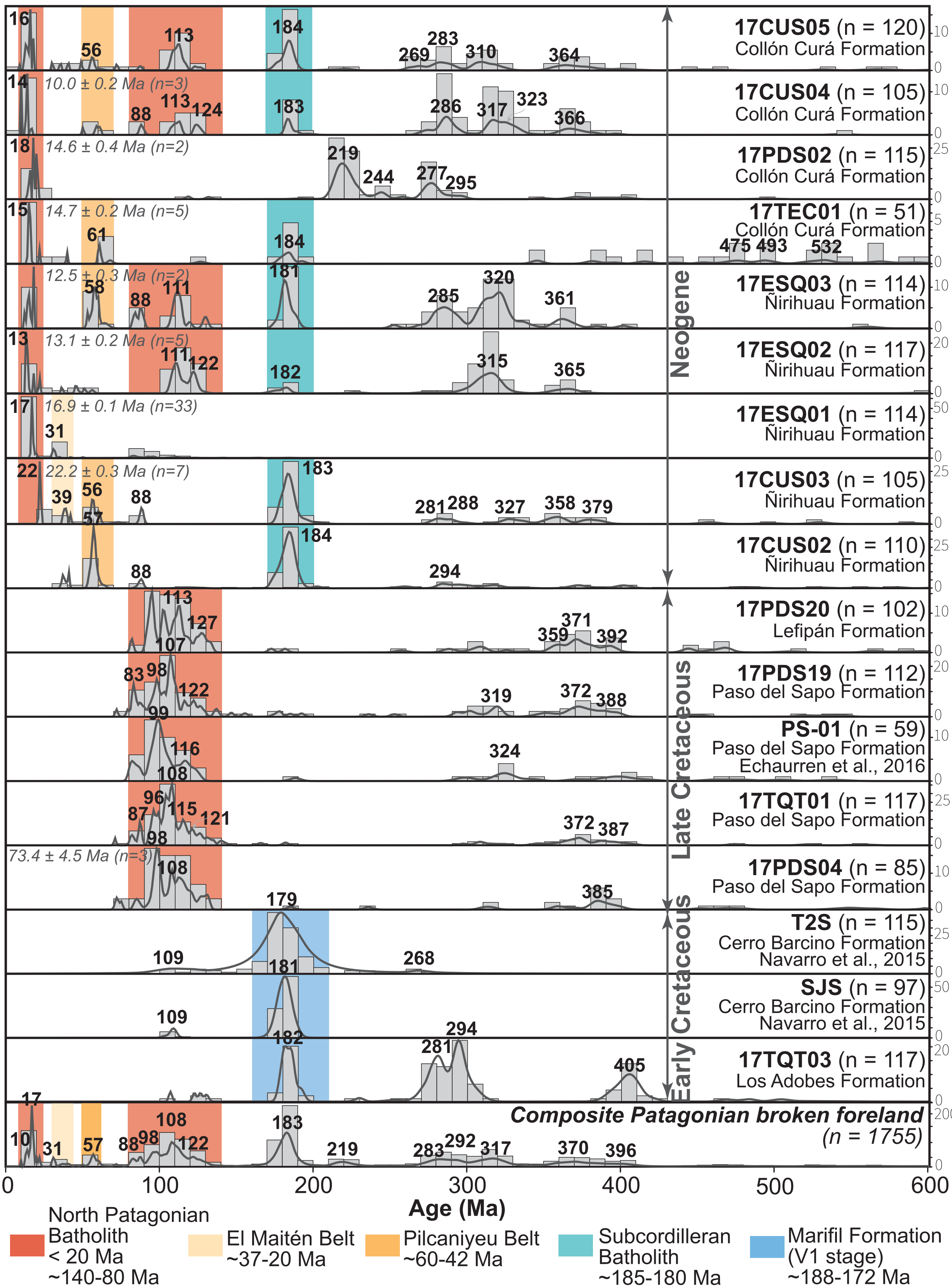

Fig. 6. Detrital zircon U-Pb age data for 17 samples of Cretaceous-Cenozoic stratigraphic units and a composite age distribution (base), shown as probability density plots (thick curves) and age histograms (thin rectangles), arranged in approximate stratigraphic order. For each age distribution, bold numerals identify age peaks (in Ma) and italicized values identify maximum depositional ages (MDAs) that may approximate true depositional ages. Shaded color rectangles identify diagnostic age populations.

Table 2
Summary table listing the maximum depositional age (MDA) on the basis of the youngest age peak, youngest single grain, or youngest 2+ grains that overlap at 2σ.

Growth structure	Growth strata position	Sample	Formation	Youngest age peak (n=)	Youngest single grain Ma ± 2σ	Youngest 2+ grains Ma ± 2σ (MSWD)	Preferred MDA Ma ± 2σ (n=)	Stratigraphic age
Cordón del Maitén	lower growth	17CUS05	Collón Curá	16 (13)	9.3 ± 0.3			Tortonian
Cordón del Maitén	pre-growth	17CUS04	Collón Curá	14 (13)	9.9 ± 0.4	10.1 ± 0.2 (0.51)	10.1 ± 0.2 (3)	Tortonian
		17PDS02	Collón Curá	18 (14)	14.5 ± 0.6	14.7 ± 0.2 (0.77)	14.6 ± 0.4 (2)	Langhian
		17TEC01	Collón Curá	15 (9)	14.5 ± 0.5		14.7 ± 0.2 (5)	Langhian
Esquel Range	lower growth	17ESQ03	Ñirihuau		12.4 ± 0.5		12.5 ± 0.3 (2)	Langhian
Esquel Range	pre-growth	17ESQ02	Ñirihuau	13 (10)	12.9 ± 0.4	13.1 ± 0.2 (0.59)	13.1 ± 0.2 (5)	Serravallian
Esquel Range	pre-growth	17ESQ01	Ñirihuau	17 (63)	16.3 ± 0.5	16.9 ± 0.1 (0.96)	16.9 ± 0.1 (33)	Burdigalian
Cordón del Maitén	lower growth	17CUS03	Ñirihuau	22 (5)	21.5 ± 1.0	22.2 ± 0.3 (1.03)	22.2 ± 0.3 (7)	Burdigalian
Cordón del Maitén	lower growth	17CUS02	Ñirihuau	41 (5)	36.4 ± 1.5	37.6 ± 2.2 (2.9)		
		17PDS20	Lefipán	82 (2)	81.4 ± 1.8			
		17PDS19	Paso del Sapo	83 (10)	71.9 ± 1.8			Mastrichtian
Taquetrén Range	lower growth	PS-01	Paso del Sapo	82 (6)	81.1 ± 3.0			Mastrichtian
		17TQT01	Paso del Sapo	87 (5)	70.9 ± 1.4			Mastrichtian
		17PDS04	Paso del Sapo	72 (3)	71 ± 2.4	73.4 ± 4.5 (3.1)	73.4 ± 4.5 (3)	Mastrichtian
		T2S	Cerro Barcino	109 (7)	102 ± 6.8	106 ± 1.6 (0.32)	106 ± 1.6 (0.32)	Albian
		SJS	Cerro Barcino	109 (7)	103 ± 2	109 ± 2.0 (0.17)	109 ± 2.0 (0.17)	Albian
		17TQT03	Los Adobes	182 (24)	106.9 ± 2.2			Albian

similar Paleozoic crystalline rocks of pre-Andean basement in the west or the North Patagonian Massif in the east (Fig. 4b).

5.2.1. Lower to mid-Cretaceous strata

For the Lower Cretaceous Chubut Group, 3 samples contain nearly unimodal U-Pb age distributions dominated by Middle Jurassic (200–180 Ma) ages and limited mid-Cretaceous (110–100 Ma) ages (Fig. 6). We interpret the vast majority of these sediments to have been derived from the Marifil Formation in distal eastern regions (Figs. 2 and 4). Navarro et al. (2015) document west-directed paleoflow within the Chubut Group, consistent with a major source in the east. However, minor contributions of mid-Cretaceous ages can only come from young or syndepositional igneous materials linked to arc magmatism associated with the North Patagonian Batholith to the west. A sample from the Los Adobes Formation (17TQT03) also contains significant Permian and Devonian populations. The Paleozoic-age zircons in the Los Adobes Formation are potentially sourced from nearby granitic basement units of the North Patagonian Massif (including the Mamil Choique and Paso del Sapo granites, and San Martín tonalite).

5.2.2. Upper Cretaceous strata

For the Upper Cretaceous to lower Paleocene Paso del Sapo and Lefipán Formations, 5 samples exhibit markedly uniform detrital zircon U-Pb age distributions (Fig. 6). In each sample, a group of mid-to Late Cretaceous grains (130–80 Ma) is dominant and provides a clear signal of derivation from Andean sources in the North Patagonian Batholith (Figs. 2 and 4). Although limited, possibly syndepositional zircon grains (Fig. 5) suggest additional input from active volcanic sources in the Andean magmatic arc. A subordinate group of Paleozoic ages spanning from roughly 400 to 300 Ma can be tied to sources of Devonian intrusive rocks and associated host rocks (Colohuincul Complex) along the eastern flank of the Andes (Hervé et al., 2013, 2016, 2018). We interpret Upper Cretaceous basin fill as derived entirely from western sources during initial growth of the North Patagonian Andes. The Late Cretaceous shift in provenance represents a basin-wide reversal in sediment polarity (Horton, 2018a), with a switch from eastern to western sources.

5.2.3. Neogene strata

Nine samples from various segments of Neogene basin fill yield the most varied U-Pb results with cosmopolitan age distributions (Fig. 6). Although there are variations among samples, most age groups can be linked to (1) the Early Jurassic Subcordilleran Batholith, (2) the Cretaceous North Patagonian Batholith, (3) Paleogene intraforeland volcanic belts, and (4) the Neogene Andean magmatic arc.

The lowermost levels of Neogene basin fill are characterized by two samples from clastic deposits considered to be the basal Ñirihuau Formation; these samples (17CUS2 and 17CUS3) are dominated by Early Jurassic grains (190-180 Ma) likely derived from the Subcordilleran Batholith, which is involved in the North Patagonian fold-thrust belt at these latitudes (Fig. 2). A subordinate late Paleocene population is unique to the Pilcaniyeu Belt (~60-42 Ma, Huitrera Formation). An upsection introduction of Oligocene to early Miocene ages is representative of the El Maitén Belt directly to the west. The youngest U-Pb ages (Fig. 5) are considered the products of syndepositional arc magmatism related to igneous activity in the North Patagonian Batholith. A broad range of roughly 400-280 Ma ages can be linked to the Colohuincul Complex and associated Devonian intrusions. Alternatively, these Paleozoic ages could be derived from the Paleozoic Accretionary Complex along the western Andean flank.

Three samples from the western exposures of the Ñirihuau Formation in the North Patagonian Andes near Esquel (samples 17ESQ01, 17ESQ02, 17ESQ03) record enhanced proportions of Paleozoic (380-270 Ma) ages, Cretaceous (120-80 Ma) ages, and syndepositional Miocene (< 20 Ma) ages (Fig. 6), which are attributed individually to derivation from pre-Andean bedrock (Colohuincul Complex and Devonian intrusions), the North Patagonian Batholith, and the active magmatic arc, respectively. All of these age groups are restricted to western source regions. Progressive upsection younging of Miocene arc-derived ages attests to continued input from a contemporaneous magmatic arc. Additional upsection trends include increases in Jurassic (Subcordilleran Belt) and Paleozoic (pre-Andean basement) ages, and the limited appearance of late Paleocene-early Eocene ages potentially derived from the Pilcaniyeu Belt.

The U-Pb results from four samples of the Collón Curá Formation show similar age signatures as the Ñirihuau Formation but in different proportions (Fig. 6). A continuous presence of Miocene grains, including syndepositional grains (Fig. 5), attests to steady volcanic input from the Andean magmatic arc. Additional age groups include Cretaceous (120-80 Ma) ages diagnostic of the North Patagonian Batholith, Jurassic ages from the Subcordilleran Batholith, and Paleozoic ages from pre-Andean units. Two samples from the easternmost Collón Curá Formation (17TEC01 and 17PDS02) are notable for the absence of Cretaceous grains, potentially the product of eastward downstream dilution by additional source materials. One of these samples (17PDS02) is further distinguished by a unique Triassic (250-210 Ma) group that is not observed in any other detrital samples in this study. This population is likely derived from intraforeland sources diagnostic of the North Patagonian Massif (Central Patagonian Batholith, Mamil Choique granite and equivalents).

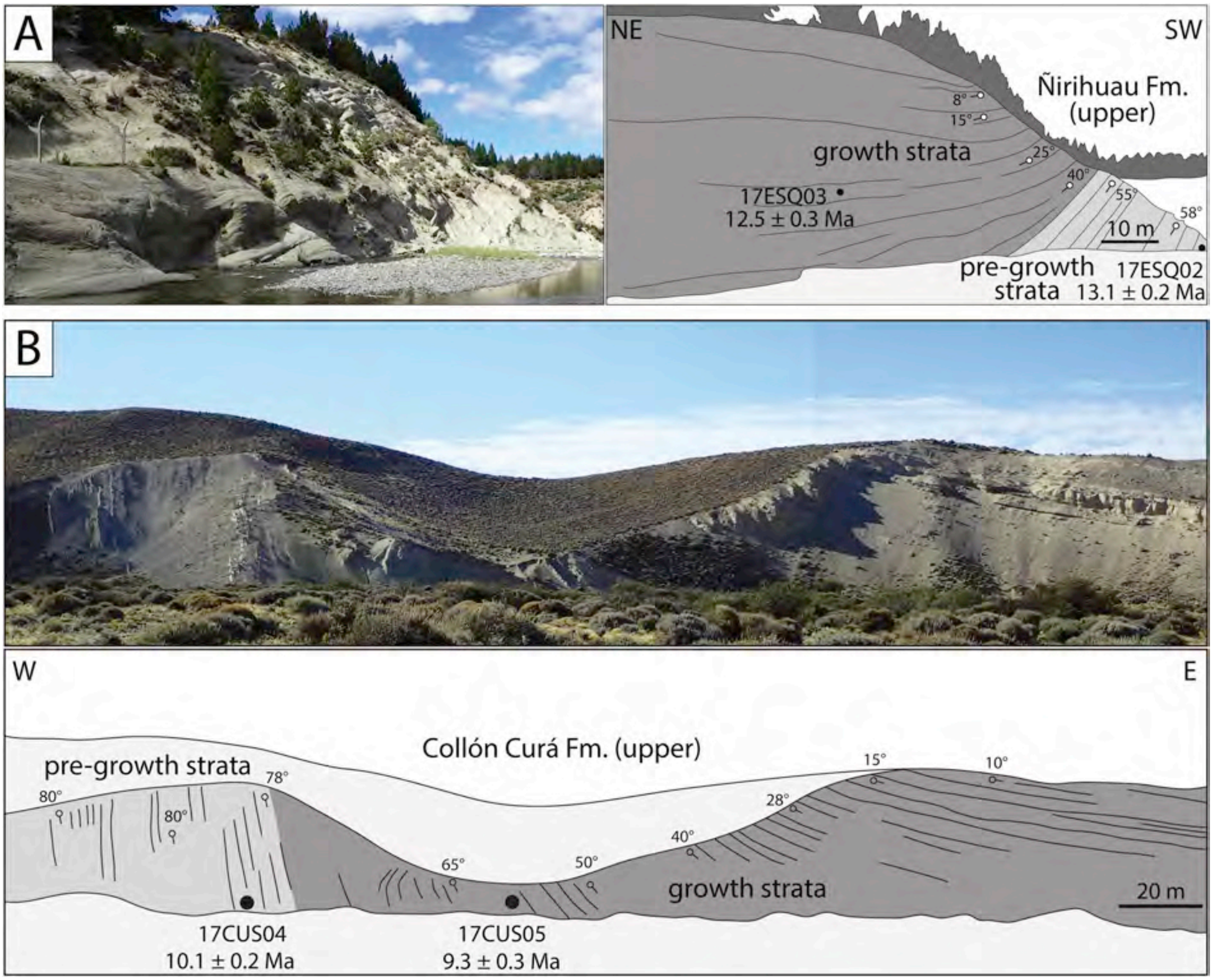

Fig. 7. Field photographs and line drawings of growth stratal packages in (A) the middle Miocene upper levels of the Ñirihuau Formation exposed in the Esquel Range of the North Patagonian foothills (after Echaurren et al., 2016) and (B) the late Miocene upper levels of the Collón Curá Formation in the broken foreland region adjacent to the Cordón del Maitén (after Ramos et al., 2015), Stratal dip values and maximum depositional ages (MDAs) for sandstone samples with young zircon U-Pb age populations (Fig. 5) are shown for pre-growth strata (light shading) and growth strata (dark shading).

Two samples from higher levels of the Collón Curá Formation, from a growth stratal succession near El Maitén (17CUS04 and 17CUS05) (Fig. 7), display perhaps the most diverse age distributions of any samples in the broken foreland (Fig. 6). These samples contain Paleozoic, Early Jurassic, Cretaceous, Paleogene, and Neogene age groups. Most of these signatures are consistent with derivation from rock units within the North Patagonian fold-thrust belt and Neogene magmatic arc to the west, similar to the Ñirihuau Formation, with the exception of Paleocene-Eocene ages likely derived from intraforeland sources of the volcanic Pilcaniyeu Belt to the north or east.

5.3. Age of growth strata

Several additional constraints arise from consideration of U-Pb results and MDAs for synorogenic basin fill associated with shortening in the fold-thrust belt and broken foreland of northern Patagonia. We highlight three cases where growth stratal relationships allow determination of the timing of activity along particular contractional structures (Table 2). These examples include the frontal segment of the fold-thrust belt in the North Patagonian Andes and the proximal (western) and distal (eastern) sectors of the broken foreland basin.

An early phase of retroarc deformation in the distal foreland is supported by U-Pb results for basin fill associated with a growth structure along the flank of the Taquetrén Range, a basement-involved uplift ~120–150 km east of the modern Andean mountain front (Fig. 2). Echaurren et al. (2016) described growth strata in the Upper Cretaceous Paso del Sapo Formation in the footwall of the southwest-directed Taquetrén thrust. From these deposits, Echaurren et al. (2016) obtained a MDA of 83.1 ± 1.6 Ma (their sample PS-01). Results presented here for three additional samples of the Paso del Sapo Formation farther west of the Taquetrén thrust show tightly clustered MDAs and single youngest grains of 72.1 ± 1.6 Ma, 71.9 ± 1.8 Ma, and 70.9 ± 1.4 Ma (17PDS04, 17PDS19, and 17TQT01). Two of these samples were collected from the basal Paso del Sapo Formation (17PDS04 and 17TQT01) approximately 40 km apart (Fig. 2); for this reason we interpret a late Campanian-Maastrichtian age of deposition and contemporaneous thrusting and structural partitioning of the Cretaceous foreland basin.

In the foothills of the North Patagonian Andes, growth strata within the Ñirihuau Formation (Fig. 7A; Echaurren et al., 2016) are associated with motion along an east-directed thrust structure responsible for uplift of the Esquel Range, a prominent north-trending range within the frontal (eastern) segment of the fold-thrust belt (Fig. 2). Samples from pre-growth and overlying growth strata yield MDAs of 13.1 ± 0.2 Ma and 12.5 ± 0.3 Ma (samples 17ESC02 and 17ESQO3) (Fig. 5). These ages indicate continuous deposition with no major hiatus during middle Miocene shortening in this foothills segment of the fold-thrust belt.

Farther east, younger growth strata within the Collón Curá Formation (Fig. 7B), identified by Ramos et al. (2015), can be linked to motion along a blind east-directed fold-thrust structure within the

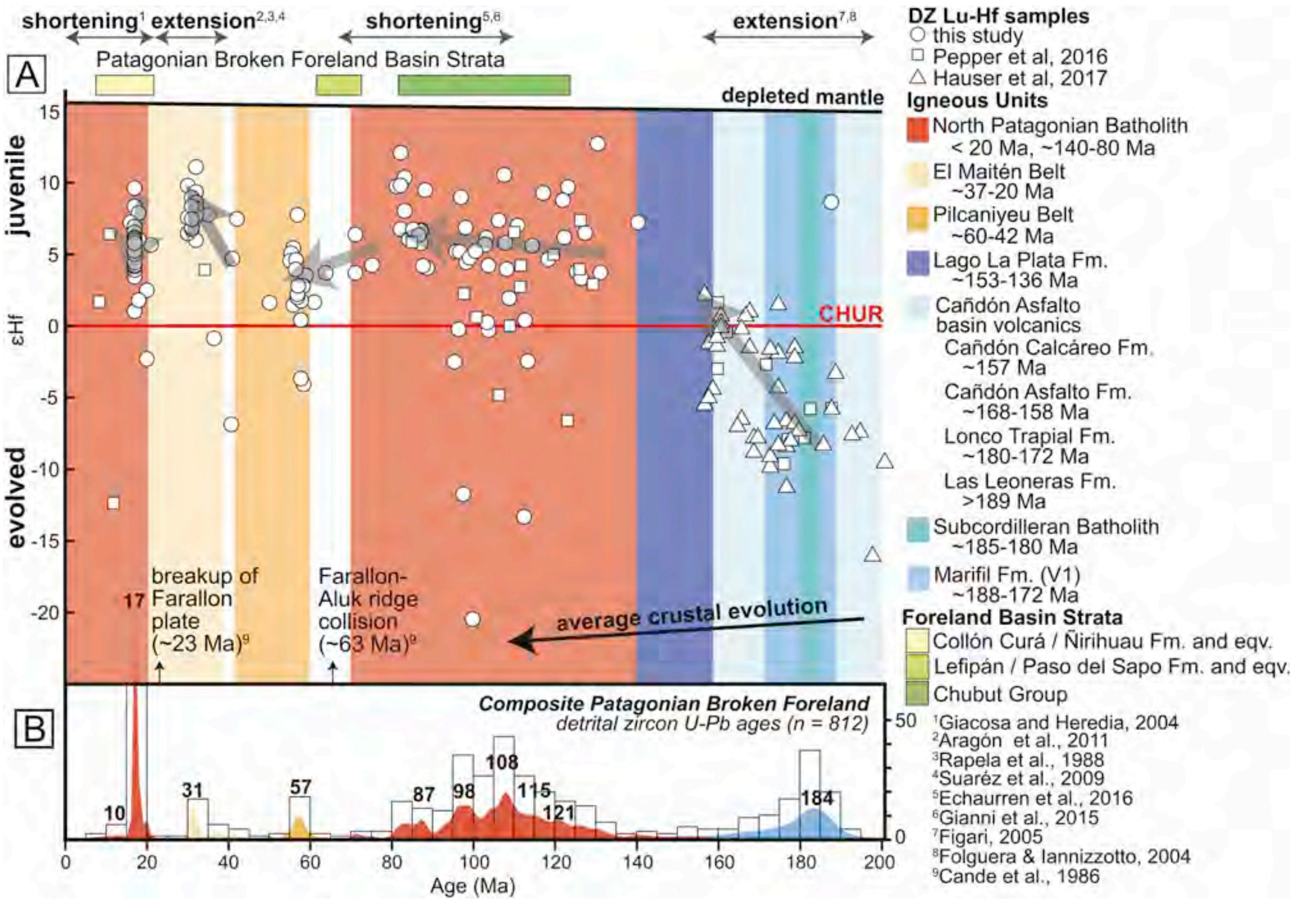

Fig. 8. (A) Hf evolution diagram and (B) corresponding detrital zircon U-Pb composite age data (below) for 200–0 Ma record in the North Patagonian broken foreland. Shaded gray arrows show running mean of the isotopic data and identify general temporal trends in Hf isotope values. CHUR = chondritic bulk reservoir. Average crustal evolution = trajectory with present-day 176Lu/177Hf = 0.0115 (Vervoort and Patchett, 1996; Vervoort and Blichert-Toft, 1999).

broken foreland region. Samples from pre-growth and overlying growth strata display youngest U-Pb ages of 10.1 ± 0.2 Ma and 9.3 ± 0.3 Ma (samples 17CUS04 and 17CUS05), respectively. These U-Pb results are slightly younger than previously reported ages of 13.5 to 11.3 Ma (Ramos et al., 2015; their samples 13-M2, MR-2, and 13-M4). These timing constraints demonstrate a late Miocene phase of shortening and further compartmentalization of the broken foreland basin. This deformation can be attributed to contractional structures responsible for uplift of the Cordón del Maitén, a north-trending range constructed during Neogene inversion of older normal faults, which originally formed during late Eocene-Oligocene extension within the El Maitén Belt and associated emplacement of widespread ignimbrites of the Ventana Formation.

6. Hf isotopic results and interpretations in the context of arc magmatism

From the detrital zircon samples, 4 samples (17PDS04, 17TQT01, 17CUS02, 17ESQ01) were selected for Hf isotope analyses in order to assess Mesozoic-Cenozoic crustal evolution and magmatic patterns from 200 to 10 Ma (e.g., Pepper et al., 2016; Balgord, 2017). A total of 130 new analyses are combined with 43 published Hf isotopic results from samples of sandstones (Hauser et al., 2017) and 26 modern river sand results (Pepper et al., 2016) into a single Hf evolution diagram (Fig. 8). The isotopic results include εHf(t) values ranging from −20 to +14 with individual mean values (for a given age) ranging from −8 to +8.

Consideration of a composite U-Pb age distribution (Fig. 8B) allows discrimination of 5 dominant age groups and corresponding Hf values: (1) 200–150 Ma, εHf(t) = -17–8 range (-8–2 mean); (2) 140–70 Ma, εHf (t) = -22–14 range (2–7 mean); (3) 60–42 Ma, εHf(t) = -5–7 range (2–5 mean); (4) 40–20 Ma, εHf(t) = -7–12 range (5–8 mean); and (5) 20–9 Ma, εHf(t) = -13–10 range (3–7 mean). These results highlight the Hf isotopic signatures of key magmatic units, including the North Patagonian Batholith, El Maitén Belt, Pilcanyeu Belt, Cañadon Asfalto Basin volcanics, and Marifil Formation. These intrusive and extrusive units have diverse magmatic affinities (Fig. 10; subduction-related, intraplate and intermediate) related to variable tectonic regimes (extension and shortening).

These records can then be compared with associated transitions in Andean magmatic arc behavior (arc advance, cessation, and retreat), on the basis of a new compilation of published isotopic ages of arc magmatism (Fig. 9). Here we highlight several key observations in the Hf isotopic record of crustal evolution (Fig. 8) and the time-space history of arc magmatism (Fig. 9), and then consider how these results support previous interpretations of the regional tectonic evolution of northern Patagonia.

(1) For the Jurassic age group, a clear trend from moderately negative to positive epsilon Hf signatures (εHf(t) = 17–8 range; -8–2 mean) indicate progressively more juvenile magmatic contributions from ~200 to 150 Ma (Fig. 8). This broadly coincided with a prolonged period of extension from the latest Triassic to earliest Cretaceous (~210-140 Ma; Rapela and Pankhurst, 1992; Folguera and Iannizzotto, 2004; Figari, 2005; Ramos, 2009) accompanied by Jurassic phases of intraplate to intermediate magmatism reflected in ~188-178 Ma lower crustal melts of the Marifil Formation and ~190-157 Ma intermediate volcanic rocks of Cañadon Asfalto Basin volcanics (Pankhurst et al., 2000; Zaffarana and Somoza,

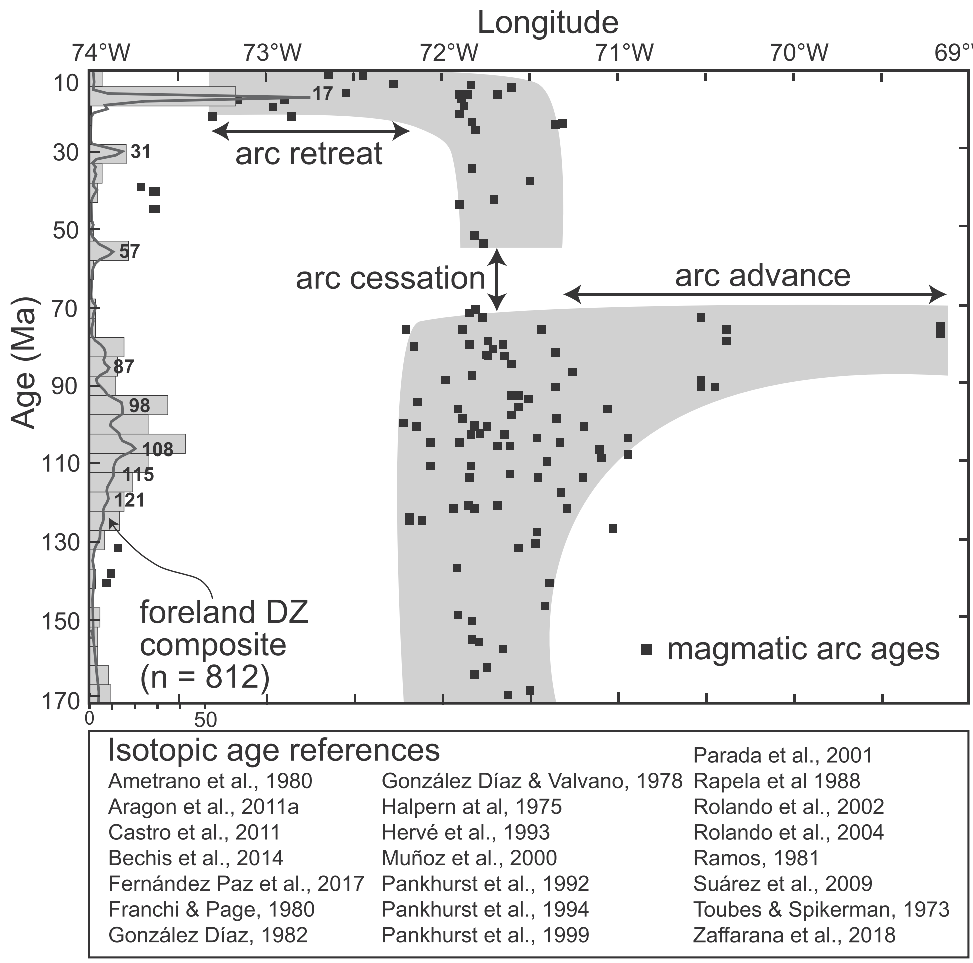

Fig. 9. Time-space plot showing the distribution of Middle Jurassic to Neogene (170–0 Ma) isotopic ages representing Andean arc magmatism at ~40–46°S. Detrital zircon U-Pb composite age data (left side) for 200–0 Ma record in the Patagonian broken foreland. Arrows denote interpreted phases of arc advance (Campanian-Maastrichtian), arc cessation (Paleocene-Eocene), and arc retreat (middle-late Miocene).

2012; Zaffarana et al., 2014). Navarrete et al. (2016) proposed that the overall extensional tectonic regime was punctuated by brief episodes of shortening (~188-185, ~170-163, ~157-136 Ma). We interpret the Jurassic trend toward increasingly positive Hf values to reflect progressively greater degrees of mantle derivation during continued crustal extension.

(2) Hf isotopic data for the Cretaceous age group (~140–70 Ma) show a broad distribution of values (εHf(t) = -22–14 range; 2–7 mean), with mostly positive (juvenile) values but an important subset of negative values indicative of considerable variation and locally evolved signatures (Fig. 8). The negative values are concentrated in the 120-90 Ma range, coincident with estimates for a late Early Cretaceous onset of shortening in northern Patagonia (Suárez et al., 2009b; 2010; Navarro et al., 2015; Echaurren et al., 2016). The Cretaceous also marks the main phase of subduction-related arc magmatism in the North Patagonian Batholith (~135-80 Ma, Pankhurst et al., 1999; Suárez and de la Cruz, 2001). We interpret these results as the products of initial Andean shortening and spatially irregular thickening of a previously thinned continental crust and lithosphere. A possible weak trend toward higher Hf values until ~90 Ma was followed by a restricted range of relatively more negative values, coeval with a Late Cretaceous phase of eastward inboard advance of the magmatic arc toward the foreland (Fig. 9), the probable result of slab flattening (Pankhurst et al., 1999; Echaurren et al., 2016, 2017).

(3) During the latest Cretaceous, a decrease in Hf isotopic values (εHf(t) = -5–7 range; 2–5 mean) immediately followed the eastward advance of the Andean magmatic arc and coincided with an apparent cessation of arc magmatism (~75-50 Ma; Figs. 8 and 9). Thereafter, a continued decrease in Hf values is expressed as Paleocene-Eocene bimodal intraplate magmatism of the Pilcaniyeu Belt (~60-42 Ma; Iannelli et al., 2017). The Hf trend is consistent with relatively more evolved signatures due to greater crustal contributions, which may reflect interactions with a thickened crust generated during Late Cretaceous shortening.

(4) A mid-Cenozoic shift to increasingly positive Hf values (εHf(t) = -7–12 range; 5–8 mean) in the 40-20 Ma time window (Fig. 8) was contemporaneous with a late Eocene–early Miocene phase of minor to moderate extension (Rapela et al., 1988; Orts et al., 2012) and associated volcanism in the El Maitén Belt (~37-20 Ma; Fernández Paz et al., 2018; Bechis et al., 2014). Although the magnitude of extension within the overriding plate is poorly constrained, we interpret this trend toward more juvenile isotopic signatures as the product of crustal thinning and greater mantle input during probable slab rollback (Horton, 2018b).

(5) During the Miocene, over the ~20-9 Ma time frame, broadly distributed Hf isotopic values (εHf(t) = -13–10 range; 1–7 mean) display a pronounced shift to lower values (Fig. 8). This signature is synchronous with the main phase of Andean shortening commencing at ~20 Ma (Giacosa and Heredia, 2004; Ramos et al., 2015; Echaurren et al., 2016), as well as renewed arc magmatism within the North Patagonian Batholith (< 20 Ma; Aragón et al., 2011b).

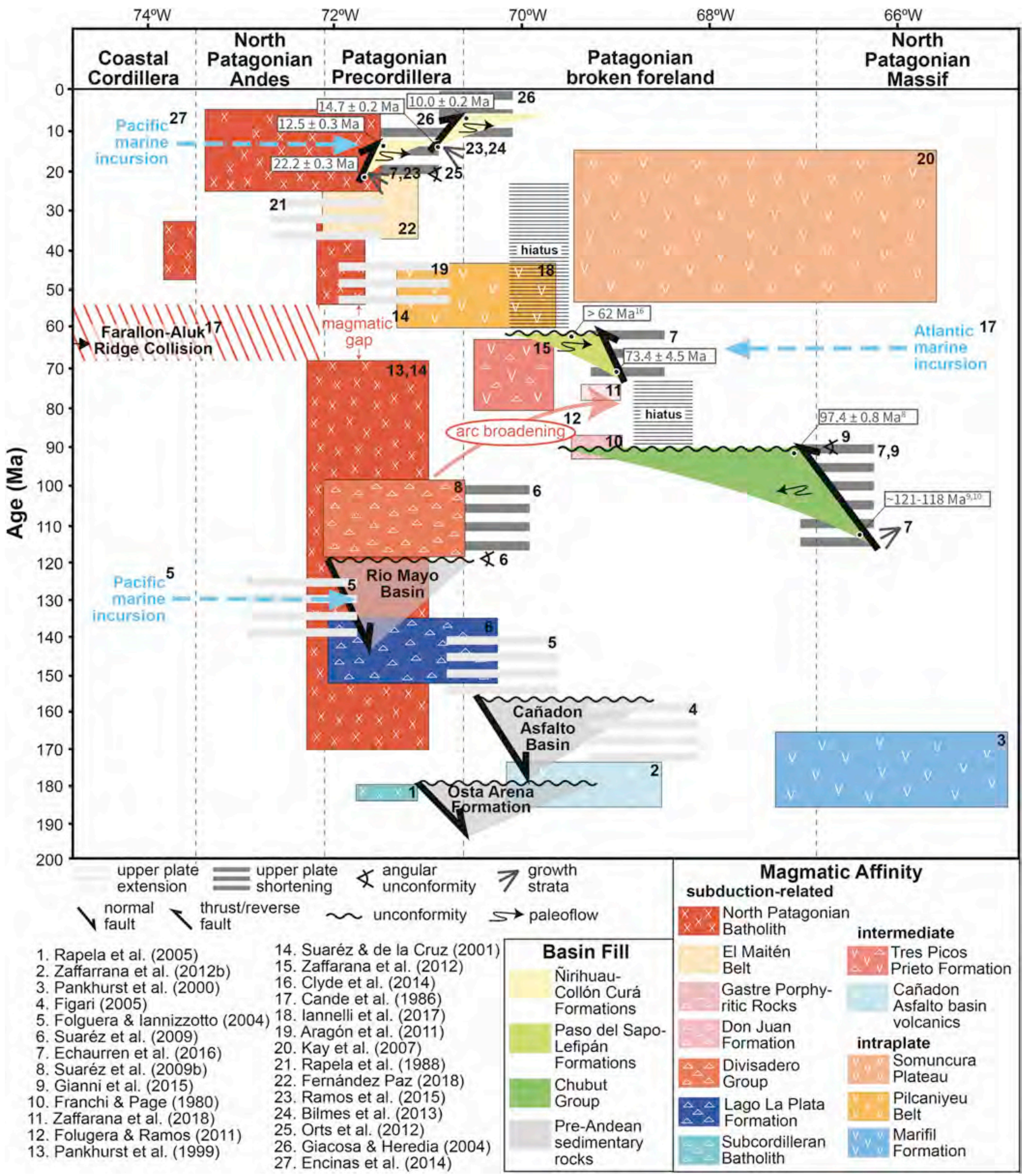

Fig. 10. Time-space plot showing the Mesozoic-Cenozoic history of northern Patagonia (~40–46°S), including arc magmatic trends, igneous affinities, deformational modes, sedimentary basin development, fault and paleoflow orientations, periods of sedimentation and non-deposition (hiatuses), and marine incursions (Encinas et al., 2014).

The more evolved signatures are consistent with Neogene crustal thickening and greater crustal interactions during enhanced magmatism. This final phase potentially coincided with arc retreat, with an apparent westward broadening of the Andean magmatic arc (Fig. 9).

7. Discussion

Accurate determinations of depositional ages and sediment provenance from detrital zircon U-Pb geochronological analyses help constrain the regional chronostratigraphic framework, timing of deformation, duration of depositional hiatuses, and inception of foreland basin sedimentation in northern Patagonia within the northern Chubut province of Argentina (42–43°S; Figs. 3, 5 and 6). A compilation of published isotopic ages demonstrates distinctive western and eastern source regions during Cretaceous–Miocene evolution of the Patagonian broken foreland basin (Fig. 4). In addition, new Hf isotopic results (Fig. 8), a synthesis of published magmatic ages (Fig. 9), and consideration of magmatic affinities and deformational modes within the overriding plate facilitate an evaluation of magmatic arc behavior and continental crustal evolution (Fig. 10).

7.1. Stratigraphic ages for the Patagonian broken foreland

The depositional ages of basin-fill units and duration of stratigraphic hiatuses are not fully resolved for the North Patagonian retroarc region. New and published detrital zircon U-Pb results indicate periods of sediment accumulation in the Aptian-Cenomanian (~106–97 Ma; Chubut Group), Campanian–early Paleocene (~74–62 Ma; Paso del Sapo and Lefipán Formations), and Miocene (~22–9 Ma; Ñirihuau, La Pava, and Collón Curá Formations), with intervening hiatuses in the Late Cretaceous (~97–74 Ma) and the late Paleocene–Oligocene (~62–22 Ma; Figs. 3 and 5).

7.2. Reversal in sediment polarity

The onset of Andean mountain building and flexural foreland subsidence can be linked to major drainage reorganization and a switch to orogenic sediment provenance (Horton, 2018a). In northern Patagonia, Jurassic to Lower Cretaceous deposits are uniformly derived from eastern sources in the North Patagonian Massif, principally from volcanic rocks of the Marifil Formation (Fig. 6), consistent with paleoflow from the east as determined by Navarro et al. (2015). A Campanian-Maastrichtian switch to western orogenic sources is recognized in the Paso del Sapo Formation, with nearly exclusive derivation from the North Patagonian Batholith and associated pre-Andean basement (Fig. 10), supported by paleoflow from the west documented by Spalletti (1996) and Scasso et al. (2012). This Late Cretaceous reversal in sediment polarity was coeval with a period of shortening and eastward advance of the magmatic arc during flat-slab subduction (Fig. 9). Sediment routing systems derived from western sources in the Andes persisted into the Neogene with dominance by the Cretaceous-Cenozoic North Patagonian Batholith, Jurassic Subcordilleran Batholith, and Paleozoic pre-Andean basement (Fig. 6). Neogene units show subordinate input from intraplate volcanic rocks to the east (Pilcaniyeu Belt), as most sediment delivered to the basin was linked to shortening-induced exhumation in the Andean fold-thrust belt and broken foreland.

7.3. Deformation timing from synorogenic growth strata

Cretaceous-Cenozoic growth strata associated with upper crustal structures constrain the timing of shortening in the Patagonian broken foreland (Fig. 10). These synorogenic deposits are associated with growth and eastward propagation of the fold-thrust belt and reactivation of inherited Jurassic normal faults, which localized basement-involved shortening in the foreland (e.g., Bilmes et al., 2013; Ramos et al., 2015; Echaurren et al., 2016). New chronostratigraphic constraints from detrital zircon U-Pb geochronology help constrain structural timing for three major growth stratal successions (Figs. 2, 5 and 7). Although Cretaceous deposits in the Andes are commonly linked to post-extensional thermal processes and the generation of regional sag basins (e.g., Uliana et al., 1989), reported growth strata within the Los Adobes and Paso del Sapo formations have been associated with reactivation of a Jurassic normal fault and uplift of pre-Jurassic basement that produced the Taquetrén Range, indicative of initial Andean shortening during Aptian(?)-Albian to Maastrichtian time (Echaurren et al., 2016).

For the Cenozoic succession, new depositional age constraints for pre-growth and growth strata refine deformational timing of contractional structures in the frontal thrust-belt foothills (Esquel Range) and proximal foreland (Cordón del Maitén; Ramos et al., 2011, 2015; Bilmes et al., 2013; Orts et al., 2012; Echaurren et al., 2016). Middle Miocene growth strata in the Ñirihuau Formation (samples 17ESQ01, 17ESQ02, and 17ESQ03) suggest that shortening in the frontal segment of the fold-thrust belt and corresponding uplift of the Esquel Range had commenced by ~13-12 Ma (Fig. 7A). Farther east, upper Miocene growth strata in the Collón Curá Formation (samples 17CUS04 and 17CUS05) suggests that shortening-related growth of the Cordón del Maitén (including possible reactivation of mid-Cenozoic extensional structures and further partitioning of the broken foreland basin) was underway at 10-9 Ma (Fig. 7B). The growth stratal relations are in accordance with available low-temperature thermochronological data, which demonstrate exhumation-related Late Cretaceous-Paleogene cooling in the broken foreland and late Miocene-Pliocene cooling along the frontal fold-thrust belt (Adriasola et al., 2005; Thomson et al., 2001; Savignano et al., 2016).

7.4. Crustal evolution and magmatism

The retroarc region of northern Patagonia recorded a complex history of varying deformational mode (shortening and extension), magmatism of diverse affinities (subduction-related, intraplate, and intermediate), and Andean magmatic arc behavior (advance/expansion, cessation, and rejuvenation; Figs. 9 and 10). Hf isotopic results elucidate crustal evolution trends that can be evaluated in the context of magmatic affinity and tectonic regime (Fig. 8).

7.4.1. Arc magmatism

Late Cretaceous broadening and eastward advance of the subduction-related magmatic arc (Figs. 9 and 10) was followed by Paleogene arc cessation in northern Patagonia (Folguera and Ramos, 2011; Gianni et al., 2018). A compilation of ~160 published magmatic arc ages at ~40–46°S support this assertion (Fig. 9; see earlier synthesis by Gianni et al., 2018). Arc broadening toward the foreland appears to have occurred at ~90–70 Ma, followed by a ~70–55 Ma period of arc shutoff. Renewed arc magmatism for the remainder of the Cenozoic and possible westward retreat occurred from ~55 to 10 Ma. Time-space variations in arc magmatism suggest a Late Cretaceous-Paleogene phase of slab shallowing (possibly to a flat-slab configuration) followed by slab resteepening during Eocene-Oligocene time (Suárez and de la Cruz, 2001; Folguera and Ramos, 2011). Such transitions in subducting slab dynamics may correlate with phases of foreland partitioning through the activation of basement-involved structures (e.g., Echaurren et al., 2016; Savignano et al., 2016; Gianni et al., 2018). Moreover, arc quiescence was partially coeval with the proposed Paleocene collision of the Farallon-Aluk ridge south of 43°30′S (Cande and Leslie, 1986; Ramos, 2005; Aragón et al., 2011b). Mid-Cenozoic renewal of arc magmatism was followed by enhanced Miocene arc magmatism in the North Patagonian Batholith, roughly coincident with plate reorganization involving breakup of the Farallon plate and subduction of the Nazca plate at ~23 Ma (Kay et al., 2007). The availability of published isotopic ages influences these interpreted patterns of arc magmatism, with particular concern over the relatively sparse sampling of more-eastern regions and Late Cretaceous magmatic units (Fig. 9).

7.4.2. Crustal evolution

To elucidate trends in crustal evolution since ~200 Ma, individual and running mean values are considered for > 200 Hf isotopic results (Fig. 8), with 130 analyses from this study and > 60 from published datasets. Five Mesozoic-Cenozoic phases are identified (Fig. 8A, gray arrows) on the basis of shifts in Hf signatures. More negative epsilon Hf values correspond to more evolved crustal signatures and more positive epsilon Hf values indicate less evolved (more juvenile) signatures.

Despite a complex history of varying deformational mode, magmatism of divergent affinities, and Andean magmatic arc behavior (Fig. 9), the identified Hf isotopic trends in crustal evolution (Fig. 8) appear to highlight several key transitions in tectonic setting (Fig. 10). (1) Phases of extension in both Jurassic (200-150 Ma) and mid-Cenozoic (40-20 Ma) produce more juvenile trajectories despite divergent magmatic affinities. (2) Phases of shortening in both the Cretaceous (120-90 Ma) and Neogene (< 20 Ma) generated more evolved values emblematic of crustal thickening. (3) Important transitions in crustal evolution may also be related to a range of processes—slab shallowing, flat-slab subduction, slab resteepening, ridge collision (and slab-window formation), and oceanic plate breakup—in operation sequentially during latest Cretaceous-Paleogene evolution of northern Patagonia.

8. Conclusions

New U-Pb and Hf isotopic results help define the chronostratigraphic framework, sediment provenance history, and crustal evolution patterns for the Patagonian broken foreland basin during geodynamic transitions in overriding plate deformational mode (shortening versus extension) and variations in subduction-related arc magmatism (advance, retreat, cessation, and rejuvenation). Detrital zircon U-Pb geochronological data help constrain the depositional ages of Cretaceous-Neogene strata, including Upper Cretaceous and Miocene growth strata linked to shortening in the fold-thrust belt (North Patagonian Andes) and to intraforeland basement uplifts (Taquetrén Range) which likely reactivate preexisting structural elements. U-Pb results also facilitate the discrimination of sediment provenance in terms of Andean sources to the west (North Patagonian Batholith, Subcordilleran Batholith, and pre-Andean basement) versus platformal sources to the east (North Patagonian Massif and intraplate volcanic units). Whereas initial retroarc deposits were originally fed by eastern sources (Chubut Group), a Late Cretaceous reversal in sedimentary polarity is defined by the nearly exclusive derivation of Campanian-Maastrichtian and younger sediments (Paso del Sapo Formation and overlying clastic strata) from the Andean magmatic arc and orogenic belt to the west.

The Patagonian broken foreland provides a detrital record of key tectonic events in the northern Chubut province of Argentina. Eastward advance of the Andean magmatic arc at ~90–70 Ma and subsequent shutoff at ~70–55 Ma is consistent with slab shallowing and subsequent flat-slab subduction. Thereafter, slab rollback coincided with a late Eocene–early Miocene phase of extension and related magmatism (El Maitén Belt) and long hiatus in foreland basin sedimentation. The Neogene depositional record (Ñirihuau and Collón Curá Formations) was governed by upper crustal shortening, renewed arc magmatism, and accumulation of clastic basin fill associated with contractional structures in the foothills of the fold-thrust belt and broken foreland farther east. The Mesozoic-Cenozoic history of variable contractional and extensional tectonic regimes is largely reflected in εHf signatures that recorded contrasting evolved and juvenile signatures during crustal thickening and thinning, respectively.

Acknowledgements

This research was funded by the U.S. National Science Foundation (Graduate Research Fellowship to Butler and grant EAR 1348031 to Horton), and research grants (to Butler) from the Geological Society of America, American Association of Petroleum Geologists, the International Association of Sedimentologists, SEPM (Society for Sedimentary Geology), and the Jackson School of Geosciences at the University of Texas at Austin. We thank Peter Flaig for field assistance, and Sarah George, Lily Jackson, Tomas Capaldi, Chelsea Mackaman-Lofland, César Navarrete, Zachary Sickmann and Gabriel Giacomone for valuable discussions. Constructive reviews from Theresa Schwartz and Andrés Bilmes improved the manuscript.

Appendices A–C. Supplementary data

Supplementary data to this article can be found online at https://doi.org/10.1016/j.jsames.2019.102242.

References

Adriasola, A.C., Thomson, S.N., Brix, M.R., Hervé, F., Stöckhert, B., 2005. Postmagmatic cooling and late cenozoic denudation of the north Patagonian batholith in the Los lagos region of Chile, 41°- 42°15S. Int. J. Earth Sci. 95, 504–528.
Alric, V., 1996. Los basaltos portadores de xenolitos aflorantes en las localidades Paso de Indios y cerro Cóndor, departamento de Paso de Indios, Provincia del Chubut. Doctoral Thesis. Universidad Nacional de la Patagonia San Juan Bosco, pp. 135.
Aragón, E., Castro, A., Díaz-Alvarado, J., Liu, D.Y., 2011a. The North Patagonian batholith at Paso Puyehue (Argentina-Chile). SHRIMP ages and compositional features. J. South Am. Earth Sci. 32, 547–554.
Aragón, E., D'Eramo, F., Castro, A., Pinotti, L., Brunelli, O.S., Rivalenti, G., Varela, R., Spakman, W., Demartis, M., Cavarozzi, C.E., Aguilera, Y.E., Mazzucchelli, M., Ribot, A., 2011b. Tectono-magmatic response to major convergence changes in the North Patagonian suprasubduction system; the Paleogene subduction–transcurrent plate margin transition. Tectonophysics 509, 218–237.
Aragón, E., Pinotti, L., Fernando, D., Castro, A., Rabbia, O., Coniglio, J., Demartis, M., Hernando, I., Cavarozzi, C.E., Aguilera, Y.E., 2013. The Farallon-Aluk ridge collision with South America: implications for the geochemical changes of slab window magmas from fore-to back-arc. Geosci. Front. 4, 377–388.
Ardolino, A., Busteros, A., Fauqué, L., Franchi, M., Lema, H., 1998. Estratigrafia del cuaternario del litoral patagonico entre Cabo Aristizabal y Bahía Camarones, Provincia del Chubut, Argentina. In: Actas X Congreso Latinoamericano de Geología y VI Congreso Nacional de Geología Económica, vol. 1. pp. 107–113.
Balgord, E.A., 2017. Triassic to Neogene evolution of the south-central Andean arc determined by detrital zircon U-Pb and Hf analysis of Neuquén Basin strata, central Argentina (34°S–40°S). Lithosphere 9, 453–462.
Balgord, E.A., Carrapa, B., 2016. basin evolution of upper cretaceous–lower cenozoic strata in the Malargüe fold-and-thrust belt: northern Neuquén basin, Argentina. Basin Res. 28, 183–206.
Bechis, F., Encinas, A., Concheyro, A., Litvak, V.D., Aguirre-Urreta, B., Ramos, V.A., 2014. New age constraints for the Cenozoic marine transgressions of northwestern Patagonia, Argentina (41°-43°S): Paleogeographic and tectonic implications. J. South Am. Earth Sci. 52, 72–93.
Biddle, K., Uliana Jr., M., Mitchum, R., Fitzgerald, M., Wright, R., 1986. The stratigraphic and structural evolution of central and eastern Magallanes Basin, Southern America. In: In: Allen, P., Homewood, P. (Eds.), Foreland Basins, vol. 8. Int. Assoc. Sedimentol. Spec. Publ., pp. 41–61.
Bilmes, A., D'Elia, L., Franzese, J.R., Veiga, G.D., Hernández, M., 2013. Miocene block uplift and basin formation in the Patagonian foreland: the Gastre Basin, Argentina. Tectonophysics 601, 98–111.
Bilmes, A., D'Elia, L., Veiga, G.D., Franzese, J.R., 2014. Relleno intermontano en el antepaís fragmentado patagónico: Evolución neógena de la cuenca de gastre. Rev. la Asoc. Geol. Argentina 71, 311–330.
Bouvier, A., Vervoort, J.D., Patchett, P.J., 2008. The Lu–Hf and Sm–Nd isotopic composition of CHUR: constraints from unequilibrated chondrites and implications for the bulk composition of terrestrial planets. Earth Planet. Sci. Lett. 273, 48–57.
Bucher, J., López, M., García, M., Bilmes, A., Elia, L.D., Funes, D., 2018. Estructura y estratigrafía de un bajo neógeno del antepaís norpatagónico : el depocentro Paso del Sapo, vol. 75. pp. 312–324 provincia de Chubut.
Cande, S.C., Leslie, R.B., 1986. Late cenozoic tectonics of the southern Chile trench. J. Geophys. Res. 91, 471–496.
Castro, A., Moreno-Ventas, I., Fernández, C., Vujovich, G., Gallastegui, G., Heredia, N., Martino, R.D., Becchio, R., Corretgé, L.G., Díaz-Alvarado, J., Such, P., García-Arias, M., Liu, D.-Y., 2011. Petrology and SHRIMP U-Pb zircon geochronology of Cordilleran granitoids of the Bariloche area, Argentina. J. South Am. Earth Sci. 32, 508–530.
Cecil, R., Gehrels, G., Patchett, J., Ducea, M., 2011. U-Pb-Hf characterization of the central Coast Mountains batholith: implications for petrogenesis and crustal architecture. Lithosphere 3, 247–260.
Cohen, K.M., Harper, D.A.T., Gibbard, P.L., 2018. ICS International Chronostratigraphic Chart 2018/08. International Commission on Stratigraphy, IUGS.
Cúneo, R., Ramezani, J., Scasso, R., Diego, P., Escapa, I., Zavattieri, A.M., Bowring, S.A., 2013. High-precision U–Pb geochronology and a new chronostratigraphy for the Cañadón Asfalto Basin, Chubut, central Patagonia: implications for terrestrial faunal and floral evolution in Jurassic. Gondwana Res. 24, 1267–1275.
Daniels, B.G., Auchter, N.C., Hubbard, S., Romans, B.W., Matthews, W.A., Stright, L., 2017. Timing of deep-water slope-evolution constrained by large-n detrital and volcanic ash zircon geochronology, Cretaceous Magallanes Basin, Chile. Geol. Soc. Am. Bull. 130, 438–454.
de Ignacio, C., López, I., Oyarzun, R., Márquez, A., 2001. The northern Patagonia Somuncura plateau basalts: a product of slab-induced, shallow asthenospheric upwelling? Terra. Nova 13, 117–121.
Dickinson, W.R., Gehrels, G.E., 2009. Use of U-Pb ages of detrital zircons to infer maximum depositional ages of strata: a test against a Colorado Plateau Mesozoic database. Earth Planet. Sci. Lett. 288 (1–2), 115–125.
Echaurren, A., Folguera, A., Gianni, G., Orts, D., Tassara, A., Encinas, A., Giménez, M., Valencia, V., 2016. Tectonic evolution of the North Patagonian Andes (41°–44° S) through recognition of syntectonic strata. Tectonophysics 677–678, 99–114.

Echaurren, A., Oliveros, V., Folguera, A., Ibarra, F., Creixell, C., Lucassen, F., 2017. Early Andean tectonomagmatic stages in north Patagonia: insights from field and geochemical data. J. Geol. Soc. Lond. 174, 405–421.
Encinas, A., Perez, F., Nielsen, S.N., Finger, K.L., Valencia, V., Duhart, P., 2014. Geochronologic and paleontologic evidence for a Pacific-Atlantic connection during the late Oligocene-early Miocene in the Patagonian Andes (43-44°S). J. South Am. Earth Sci. 55, 1–18.
Fernández Paz, L., Litvak, V.D., Echaurren, A., Iannelli, S.B., Encinas, A., Folguera, A., Valencia, V., 2018. Late Eocene volcanism in north Patagonia (42°30′–43°S): arc resumption after a stage of within-plate magmatism. J. Geodyn. 113, 13–31.
Figari, E.G., 2005. Evolución tectónica de la Cuenca de Cañadón Asfalto (Zona del valle medio del Río Chubut). Ph.D. thesis. Universidad de Buenos Aires.
Figari, E.G., Scasso, R.A., Cúneo, R.N., Escapa, I., 2015. Estratigrafía y evolución geológica de la Cuenca de Cañadón Asfalto , Provincia del Chubut , Argentina. Lat. Am. J. Sedimentol. Basin Anal. 22.
Folguera, A., Encinas, A., Alvarez, O., Orts, D., Gianni, G., Echaurren, A., Litvak, V.D., Navarrete, C., Sellés, D., Tobal, J., Ramos, M., Fennell, L., Fernández, L., Giménez, M., Martínez, P., Ruiz, F., Iannelli, S., 2018a. Neogene growth of the Patagonian Andes. In: Folguera, A. (Ed.), The Evolution of the Chilean-Argentinean Andes. Springer Earth System Sciences. Springer, Cham, pp. 485–511.
Folguera, A., Encinas, A., Echaurren, A., Gianni, G., Orts, D., Valencia, V., Carrasco, G., 2018b. Constraints on the Neogene growth of the central Patagonian Andes at the latitude of the Chile triple junction (45°-47°S) using U/Pb geochronology in synorogenic strata. Tectonophysics 744, 134–154.
Folguera, A., Iannizzotto, N.F., 2004. The lagos La Plata and Fontana fold-and-thrust belt: long-lived orogenesis at the edge of western Patagonia. J. South Am. Earth Sci. 16, 541–566.
Folguera, A., Ramos, V.A., 2011. Repeated eastward shifts of arc magmatism in the Southern Andes: a revision to the long-term pattern of Andean uplift and magmatism. J. South Am. Earth Sci. 32, 531–546.
Fosdick, J.C., Romans, B.W., Fildani, A., Bernhardt, A., Calderón, M., Graham, S.A., 2011. Kinematic evolution of the Patagonian retroarc fold-and-thrust belt and Magallanes foreland basin, Chile and Argentina, 51°30'S. Geol. Soc. Am. Bull. 123, 1679–1698.
Franchi, M.R., Page, R., 1980. Los basaltos cretácicos y la evolución magmática del Chubut Occidental. Rev. Asoc. Geol. Argent. 35, 208–229.
Franzese, J.R., D'Elia, L., Bilmes, A., Bucher, J., García, M., López, M., Muravchik, M., Hernández, M., 2018. Evolution of a Patagonian Miocene intermontane basin and its relationship with the Anean foreland: Tectono-stratigraphic evidences from the catán Lil basin, Argentina. J. South Am. Earth Sci. 86, 162–175.
Franzese, J., Spalletti, L., Pérez, I.G., Macdonald, D., 2003. Tectonic and paleoenvironmental evolution of Mesozoic sedimentary basins along the Andean foothills of Argentina (32–54 S). J. South Am. Earth Sci. 16, 81–90.
García Morabito, E., Ramos, V.A., 2012. Andean evolution of the Aluminé fold and thrust belt, northern Patagonian Andes (38°30'-40°30'S). J. South Am. Earth Sci. 38, 13–30.
Gehrels, G.E., Valencia, V., Pullen, A., 2006. Detrital zircon geochronology by laser-ablation multicollector ICPMS at the Arizona LaserChron center. In: In: Loszewski, T., Huff, W. (Eds.), Geochronology: Emerging Opportunities, Paleontology Society Short Course: Paleontology Society Papers, vol. 11. pp. 1–10.
Gehrels, G.E., Valencia, V., Ruiz, J., 2008. Enhanced precision, accuracy, efficiency, and spatial resolution of U-Pb ages by laser ablation–multicollector–inductively coupled plasma– mass spectrometry. Geochem. Geophys. Geosyst. 9.
Gehrels, G., Pecha, M., 2014. Detrital zircon U-Pb geochronology and Hf isotope geochemistry of Paleozoic and Triassic passive margin strata of western North America. Geosphere 10, 49–65.
Ghiglione, M.C., Quinteros, J., Yagupsky, D., Bonillo-Martínez, P., Hlebszevtich, J., Ramos, V.A., Vergani, G., Figueroa, D., Quesada, S., Zapata, T., 2010. Structure and tectonic history of the foreland basins of southernmost South America. J. South Am. Earth Sci. 29, 262–277.
Giacosa, R.E., Heredia, N., 2004. Structure of the North Patagonian thick-skinned fold-and-thrust belt, southern central Andes, Argentina (41°–42°S). J. South Am. Earth Sci. 18, 61–72.
Giacosa, R.E., Afonso, J.C., Heredia, N., Paredes, J., 2005. Tertiary tectonics of the sub-Andean region of the North Patagonian Andes, southern central Andes of Argentina (41–42°S30'S). J. South Am. Earth Sci. 20, 157–170.
Gianni, G., Navarrete, C., Orts, D., Tobal, J., Folguera, A., Giménez, M., 2015. Patagonian broken foreland and related synorogenic rifting: the origin of the Chubut Group Basin. Tectonophysics 649, 81–99.
Gianni, G.M., Dávila, F.M., Echaurren, A., Fennel, L., Tobal, J., Navarrete, C., Quezada, P., Folguera, A., Giménez, M., 2018. A geodynamic model linking Cretaceous orogeny, arc migration, foreland dynamic subsidence and marine ingression in southern South America. Earth Sci. Rev. 185, 437–462.
Gonzánlez Díaz, E.F., 1982. Chronological zonation of granitic plutonism in the Northern Patagonian Andes of Argentina: the migration of intrusive cycles. Earth Sci. Rev. 18, 365–393.
Hauser, N., Cabaleri, N.G., Gallego, O.F., Monferran, M.D., Silva Nieto, D., Armella, C., Matteini, M., Aparicio González, P.A., Pimentel, M.M., Volkheimer, W., Reimold, W.U., 2017. U-Pb and Lu-Hf zircon geochronology of the Cañadón Asfalto Basin, Chubut, Argentina: implications for the magmatic evolution in central Patagonia. J. South Am. Earth Sci. 78, 190–212.
Hervé, F., 1994. The southern Andes between 39° and 44° S latitude: the geological signature of a transpressive tectonic regime related to a magmatic arc. In: Reutter, K.J., Scheuber, E., Wigger, P. (Eds.), Tectonics of the Southern Central Andes. Springer-Verlag, Berlin, pp. 243–248.
Hervé, F., Calderón, M., Fanning, C.M., Pankhurst, R.J., Fuentes, F., Rapela, C.W., Correa, J., Quezada, P., Marambio, C., 2016. Devonian magmatism in the accretionary complex of southern Chile. J. Geol. Soc. Lond. 173, 587–602.
Hervé, F., Calderón, M., Fanning, C.M., Pankhurst, R.J., Godoy, E., 2013. Provenance variations in the Late Paleozoic accretionary complex of central Chile as indicated by detrital zircons. Gondwana Res. 23, 112–113.
Hervé, F., Calderón, M., Fanning, M., Pankhurst, R.J., Rapela, C.W., Quezada, P., 2018. The country rocks of Devonian magmatism in the north Patagonian massif and Chaitenia. Andean Geol. 45, 301–317.
Horton, B.K., Fuentes, F., 2016. Sedimentary record of plate coupling and decoupling during growth of the Andes. Geology 44, 647–650.
Horton, B.K., Fuentes, F., Boll, A., Starck, D., Ramirez, S.G., Stockli, D.F., 2016. Andean stratigraphic record of the transition from backarc extension to orogenic shortening: a case study from the northern Neuquén Basin, Argentina. J. South Am. Earth Sci. 71, 17–40.
Horton, B.K., Perez, N.D., Fitch, J.D., Saylor, J.E., 2015. Punctuated shortening and subsidence in the Altiplano plateau of southern Peru: implications for early Andean mountain building: Lithosphere. 7, 117–137.
Horton, B.K., 2018a. Sedimentary record of Andean mountain building. Earth Sci. Rev. 178, 279–309. https://doi.org/10.1016/j.earscirev.2017.11.025.
Horton, B.K., 2018b. Tectonic regimes of the central and southern Andes: responses to variations in plate coupling during subduction. Tectonics 37, 402–429. https://doi.org/10.1002/2017TC004624.
Howell, J.A., Schwarz, E., Spalletti, L.A., Veiga, G.D., 2005. The Neuquén basin: an overview. Geol. Soc. Lond. Spec. Publ. 252, 1–14.
Iannelli, S.B., Fennell, L.M., Litvak, V.D., Fernández, P.L., Encinas, A., Folguera, A., 2018. Geochemical and tectonic evolution of late cretaceous to early Paleocene magmatism along the southern central Andes (35-36 S). J. South Am. Earth Sci. 87, 139–156.
Iannelli, S.B., Litvak, V.D., Fernandez Paz, Folguera, A., Ramos, M.E., Ramos, V.A., 2017. Evolution of Eocene to Oligocene arc-related volcanism in the north Patagonian Andes (39-41°S), prior to the break up of the Farallon plate. Tectonophysics 696–697, 70–87.
Jordan, T.E., Burns, W.M., Veiga, R., Pángaro, F., Copeland, P., Kelley, S., Mpodozis, 2001. Extension and basin formation in the southern Andes caused by increased convergence rate: a mid-Cenozoic trigger for the Andes. Tectonics 20, 234–308.
Kay, S.M., Ardolino, A.A., Gorring, M.L., Ramos, V.A., 2007. The Somuncura large igneous province in Patagonia: interaction of a transient mantle thermal anomaly with a subducting slab. J. Petrol. 48, 43–77.
Lizuaín, A., Viera, R., 2010. Descripción geológica de la Hoja 4372-I y II, Esquel, Provincia de Chubut, vol. 369. Servicio Geológico Minero Argentino, Instituto de Geología y Recursos Minerales, Boletín, pp. 1–92.
Ludwig, K.R., 2008. Isoplot/Ex 3.70: A Geochronological Toolkit for Microsoft Excel, vol. 4. Berkley Geochronologic Center Special Publication, pp. 1–77.
López, Manuel, García, Micaela, Bucher, Joaquin, Daniela, S. Funes, D'Elia, Leandro, Bilmes, Andrés, Naipauer, Maximiliano, Ana, M. Sato, Valencia Victor, A., Franzese, Juan, August 2019. Structural evolution of the Collón Cura basin: tectonic implications for the North Patagonian broken foreland. J. South Am. Earth Sci. 93, 424–438.
Marveggio, N., Llorens, M., 2013. Nueva edad de la base del Grupo Chubut en la mena uranífera Cerro Solo, provincia del Chubut. Rev. Asoc. Geol. Argent. 70, 318–326.
Mazzoni, M., Kawashita, K., Harrison, S., Aragón, E., 1991. Edades radimetricas eocenas, Borde Occidental del Macizo Norpatagonico. Rev. Asoc. Geol. Argent. 46, 150–158.
Muñoz, J., Araneda, M., McDonough, M., 1998. Geofísica regional. In: SERNAGEOMIN, 1998. Estudio Geológico-Económico de la X Región Norte (Inédito), Servicio Nacional de Geología y Minería, Informe Registrado IR-15-98pp. 6.
Muñoz, J., Troncoso, R., Dunhart, P., Crignola, P., Farmer, L., Stern, C.R., 2000. The relation of the mid-Tertiary coastal magmatic belt in south-central Chile to the late Oligocene increase in convergence rate. Rev. Asoc. Geol. Argent. 27, 1–23.
Navarro, E.L., Astini, R.A., Belousova, E., Guler, M.V., Gehrels, G., 2015. Detrital zircon geochronology and provenance of the Chubut Group in the northeast of Patagonia, Argentina. J. South Am. Earth Sci. 63, 149–161.
Navarrete, C., Gianni, G., Echaurren, A., Kingler, F.L., Folguera, A., 2016. Episodic Jurassic to lower cretaceous intraplate compression in central Patagonia during Gondwana breakup. J. Geodyn. 102, 185–201. https://doi.org/10.1016/j.jog.2016.10.001.
Orts, D., Folguera, A., Encinas, A., Ramos, M., Tobal, J., Ramos, V.A., 2012. Tectonic development of the North Patagonian Andes and their related Miocene foreland basin (41°30′-43°S). Tectonics 31, TC3012. https://doi.org/10.1029/2011TC003084.
Orts, D.L., Folguera, A., Giménez, M., Ruiz, F., Rojas Vera, E.A., Klinger, F.L., 2015. Cenozoic building and deformational processes in the north Patagonian Andes. J. Geodyn. 86, 26–41.
Pankhurst, R.J., Hervé, F., Rapela, C.W., 1994. Sm-Nd evidence for the Grenvillian provenance of the metasedimentary basement of Southern Chile and West Antarctica. In: 7° Congreso Geológico Chileno, Concepción, Actas, vol. 2. pp. 1414–1418.
Pankhurst, R.J., Rapela, C.R., 1995. Production of Jurassic rhyolite by anatexis of the lower crust of Patagonia. Earth Planet. Sci. Lett. 134, 23–36.
Pankhurst, R.J., Rapela, C.W., Fanning, C.M., Márquez, M., 2006. Gondwanide continental collision and the origin of Patagonia. Earth Sci. Rev. 76, 235–257.
Pankhurst, R.J., Riley, T.R., Fanning, C.M., Kelley, S.P., 2000. Episodic silicic volcanism in Patagonia and Antarctic peninsula: chronology of the magmatism associated with the break-up of Gondwana. J. Petrol. 41, 605–625.
Pankhurst, R.J., Weaver, S.D., Hervé, F., Larrondo, P., 1999. Mesozoic-cenozoic evolution of the north Patagonian batholith in Aysén, southern Chile. J. Geol. Soc. Lond. 156, 673–694.
Pepper, M., Gehrels, G., Pullen, A., Ibanez-Mejia, M., Ward, K.M., Kapp, P., 2016. Magmatic history and crustal genesis if western South America: constraints from U-Pb ages and Hf isotopes of detrital zircons in modern rivers. Geosphere 12, 1532–1555.
Ramos, V., 2005. Seismic ridge subduction and topography: foreland deformation in the Patagonian Andes. Tectonophysics 399, 73–86.

Ramos, V.A., 2008. Patagonia: a paleozoic continent adrift? J. South Am. Earth Sci. 26, 235–251.
Ramos, V.A., 2009. Anatomy and global context of the Andes: main geologic features and the orogenic cycle. In: In: Kay, S.M., Ramos, V.A., Dickinson, W.R. (Eds.), Backbone of the Americas: Shallow Subduction, Plateau Uplift, and Ridge and Terrane Collision: Geol, vol. 204. Soc. Am. Mem, pp. 31–65.
Ramos, M.E., Orts, D., Calatayud, F., Pazos, P.J., Folguera, A., Ramos, V., 2011. Estructura, estratigrafía y evolución tectónica de la cuenca de Ñirihuau en las Nacientes del Río Cushamen, Chubut 68. pp. 210–224.
Ramos, M.E., Tobal, J.E., Sagripanti, L., Folguera, A., Orts, D.L., Giménez, M., Ramos, V.A., 2015. The North Patagonian orogenic front and related foreland evolution during the Miocene, analyzed from synorogenic sedimentation and U/Pb dating (~42°S). J. South Am. Earth Sci. 64, 467–485.
Rapela, C.W., Pankhurst, R.J., 1992. The granite of northern Patagonia and the gastre fault system in relation to the break-up of Gondwana. In: In: Storey, B.C., Alabaster, T., Pankhurst, R.J. (Eds.), Magmatism and the Causes of Continental Break-Up, vol. 68. Geol. Soc. London, Spec. Publ., pp. 209–220.
Rapela, C.W., Spalletti, L.A., Merodio, J.C., Aragón, E., 1988. Temporal evolution and spatial variation of early Tertiary volcanism in the Patagonian Andes (40°S-42°30'S). J. South Am. Earth Sci. 1, 75–88.
Rapela, C.W., Pankhurst, R.J., Harrison, S.M., 1992. Triassic "Gondwana" granites of the Gastre district. North Patagonian Massif. Trans. Royal Soc. Edinb. Earth Sci. 84, 291–304.
Rapela, C.W., Pankhurst, R.J., Fanning, C.M., Hervé, F., 2005. Pacific subduction coeval with the Karoo mantle plume: the Early Jurassic Subcordilleran belt of northwestern Patagonia. In: In: Vaughan, A.P.M., Leat, P.T., Pankhurst, R.J. (Eds.), Terrane Processes at the Margins of Gondwana, vol. 246. Geological Society, London, Special Publications, pp. 217–239.
Rolando, A., Hartmann, L., Orestes, J., Fernández, R., Etcheverry, R., Schalamuk, I., McNaughton, N., 2002. SHRIMP zircon U-Pb evidence for extended Mesozoic magmatism in the Patagonian Batholith and assimilation of Archean crustal components. J. South Am. Earth Sci. 15, 267–283.
Rolondo, A.P., Hartmann, L.A., Santos, J.O., Fernandez, R.P., Etcheverry, R.O., Schalamuk, I.A., 2004. McNaughton, SHRIMP U-Pb zircon dates from igneous rocks from the Fontana Lake region, Patagonia: Implications forthe age of magmatism, Mesozoic geological evolution and age of basement. Revista de la Asociación Geológica Argentina 59, 671–684.
Romans, B.W., Hubbard, S.M., Covault, J.A., Fosdick, J.C., Graham, S.A., 2011. Evolution of deep-water stratigraphic architecture, Magallanes Basin, Chile. Mar. Pet. Geol. 28, 612–628.
Savignano, E., Mazzoli, S., Arce, M., Franchini, M., Gautheron, C., Paolini, M., Zattin, M., 2016. (Un)Coupled thrust belt-foreland deformation in the northern Patagonian Andes: new insights from the Esquel-Gastre sector (41°30′–43°S). Tectonics 35, 2636–2656.
Scasso, R.A., Alberhan, M., Ruiz, L., Weidemeyer, S., Medina, F.A., Kiessling, W., 2012. Integrated bio- and lithofacies analysis of coarse-grained, tide-dominated deltaic environments across the Cretaceous/Paleogene boundary in Patagonia, Argentina. Cretac. Res. 36, 37–57.
Schwartz, T.M., Fosdick, J.C., Graham, S.A., 2017. Using detrital zircon U-Pb ages to calculate Late Cretaceous sedimentation rates in the Magallanes-Austral basin, Patagonia. Basin Res. 29, 725–746.
Spalletti, L.A., 1996. Estuarine and shallow-marine sedimentation in the upper cretaceouse lower Tertiary west-central Patagonian Basin (Argentina). In: In: de Batist, M., Jacobs, P. (Eds.), Geology of Siliciclastic Shelf Seas, vol. 117. Geol. Soc. London, Spec. Publ., pp. 81–93.
Spalletti, L.A., Dalla Salda, L.H., 1996. A pull apart volcanic related Tertiary basin, an example from the Patagonian Andes. J. South Am. Earth Sci. 9, 197–206.
Suárez, M., de la Cruz, R., 2001. Jurassic to Miocene K–Ar dates from eastern central Patagonian Cordillera plutons, Chile (45°–48° S). Geol. Mag. 183, 53–66.
Suárez, M., De La Cruz, R., Bell, M., Demant, A., 2010. Cretaceous slab segmentation in southwestern Gondwana. Geol. Mag. 147, 193–205.
Suárez, M., De la Cruz, R., Aguirre-Urreta, B., Fanning, M., 2009a. Relationship between volcanism and marine sedimentation in northern Austral (Aisén) Basin, central Patagonia: stratigraphic, U–Pb SHRIMP and paleontologic evidence. J. South Am. Earth Sci. 27, 309–325.
Suárez, M., Marquez, M., De La Cruz, R., Fanning, M., 2009b. Aptian-Albian Subaerial Volcanic Rocks in Central Patagonia: Divisadero and Chubut Groups. XII Congreso Geológico Chileno, Santiago.
Suárez, M., Márquez, M., De La Cruz, R., Navarrete, C., Fanning, M., 2014. Cenomanian-? early Turonian minimum age of the Chubut Group, Argentina: SHRIMP U-Pb geochronology. J. South Am. Earth Sci. 50, 67–74.
Thomson, S.N., 2002. Late Cenozoic geomorphic and tectonic evolution of the Patagonian Andes between latitudes 42°S and 46°S: an appraisal based on fission-track results from the transpressional intra-arc Liquiñe-Ofqui fault zone. Geol. Soc. Am. Bull. 114, 1159–1173.
Thomson, S.N., Hervé, F., Stöckhert, B., 2001. Mesozoic-Cenozoic denudation history of the Patagonian Andes (southern Chile) and its correlation to different subduction processes. Tectonics 20, 693–711.
Uliana, M.A., Biddle, K.T., Cerdan, J., 1989. Mesozoic extension and the formation of Argentine sedimentary basins. Am. Assoc. Pet. Geol. Mem. 46, 599–614.
Vervoort, J.D., Patchett, P.J., 1996. Behavior of hafnium and neodymium isotopes in the crust: constraints from Precambrian crustally derived granites. Geochim. Cosmochim. Acta 60, 3717–3733.
Vervoort, J.D., Blichert-Toft, J., 1999b. Evolution of the depleted mantle: Hf isotope evidence from juvenile rocks through time. Geochim. Cosmochim. Acta 63, 533–556.
Wilf, P., Singer, B.S., Zamaloa, M., Johnson, K.R., Cúneo, N.R., 2010. Early Eocene 40Ar/39Ar age for the Pampa de Jones plant, frog, and insect biota (Huitrera Formation, Neuquén province, Patagonia, Argentina). AMEGHINIANA Rev. Asoc. Paleontol. Argent. 47, 207–216.
Zaffarana, C., Lagorio, S., Orts, D., Busteros, A., Nieto, D.S., Giacosa, R., Gonzalez, V.R., Bolthauser, B., Negre, C.P., Somoza, R., Haller, M., 2018. First geochemical and geochronological characterization of Late Cretaceous mesosilicic magmatism in Gastre, Northern Patagonia, and its tectonic relation to other coeval volcanic rocks in the region. Geol. Mag. https://doi.org/10.1017/S0016756818000432.
Zaffarana, C.B., Lagorio, S.L., Somoza, R., 2012. Paleomagnetism and geochemistry from the upper cretaceous Tres Picos Prieto locality (43°S), Patagonian plateau basalts. Andean Geol. 39, 53–66.
Zaffarana, C.B., Somoza, R., 2012. Palaeomagnetism and 40Ar/39Ar dating from Lower Jurassic rocks in Gastre, central Patagonia: further data to explore tectonomagmatic events associated with the break-up of Gondwana. J. Geol. Soc. Lond. 169, 371–379.
Zaffarana, C.B., Somoza, R., López de Luchi, M., 2014. The late Triassic central Patagonian batholith: magma hybridization, 40Ar/39Ar ages and thermobarometry. J. South Am. Earth Sci. 55, 94–122.